MNRAS **000**, 1–24 (2019) Preprint 6 April 2020 Compiled using MNRAS LATEX style file v3.0

The SDSS/APOGEE Catalog of HgMn Stars

S. Drew Chojnowski,[1]⋆ Swetlana Hubrig,[2] Sten Hasselquist,[3,4] Rachael L. Beaton,[5] Steven R. Majewski,[6] D. A. García-Hernández,[7,8] and David DeColibus,[1]

[1] *Apache Point Observatory and New Mexico State University, P.O. Box 59, Sunspot, NM, 88349-0059, USA*
[2] *Leibniz-Institut für Astrophysik Potsdam (AIP), An der Sternwarte 16, 14482 Potsdam, Germany*
[3] *Department of Physics & Astronomy, University of Utah, 115 1400 E, Salt Lake City, UT 84112, USA*
[4] *NSF Astronomy and Astrophysics Postdoctoral Fellow*
[5] *The Observatories of the Carnegie Institution for Science, 813 Santa Barbara Street, Pasadena, CA 91101, USA*
[6] *Department of Astronomy, University of Virginia, P.O. Box 400325, Charlottesville, VA 22904-4325, USA*
[7] *Instituto de Astrofísica de Canarias (IAC), E-38205 La Laguna, Tenerife, Spain*
[8] *Universidad de La Laguna (ULL), Departamento de Astrofísica, E-38206 La Laguna, Tenerife, Spain*

Accepted XXX. Received YYY; in original form ZZZ

ABSTRACT

We report on *H*-band spectra of chemically peculiar Mercury-Manganese (HgMn) stars obtained via the SDSS/APOGEE survey. As opposed to other varieties of chemically peculiar stars such as the hotter He-strong and the usually cooler classical Ap/Bp stars, HgMn stars lack strong magnetic fields and are defined by their extreme overabundances of Hg and Mn, along with other heavy elements such as Xe, Pt, and Au. A satisfactory explanation for the abundance patterns remains to be determined, but low rotational velocity is a requirement and involvement in binary/multiple systems may be as well. The APOGEE HgMn sample currently consists of 269 stars that were identified among the APOGEE telluric standard star sample as those whose metallic absorption content is limited to or dominated by the *H*-band Mn II lines. Due to the fainter magnitudes probed by the APOGEE survey as compared to past studies, only 9/269 stars in the sample were previously known as HgMn types. The rest of the stars are identified as HgMn stars for the first time, thus more than doubling the known sample of HgMn stars. At least 32% of the APOGEE sample are found to be binary or multiple systems, and from multi-epoch spectroscopy, we were able to determine orbital solutions for at least one component in 32 binaries. Many of the double-lined and triple-lined systems include chemically peculiar secondary stars, with noteworthy examples being the HgMn+Ap/Bp binary 2MASS J00570626+6134007 (HD 5429), the HgMn+HgMn binary 2MASS J09432220−5348264 (HD 298641), and the HgMn+Bp Mn+Am triple system 2MASS J19223868+1433117 (HD 231263). As a further peculiarity, roughly half of the sample produces narrow emission in the C I 16895 Å line, with widths and radial velocities that match those of the Mn II lines.

Key words: stars: chemically peculiar – stars: variables:

1 INTRODUCTION

Whereas strong magnetic fields are the cause of the chemical peculiarities in classical Ap/Bp stars, the origin of the occasionally extreme heavy metal abundances in HgMn stars remains to be determined. The HgMn stars are typically defined by their optical spectra, in which overabundances of Hg (up to 6 dex over Solar; e.g., White, et al. 1976) and Mn (up to 3 dex over Solar; e.g., Smith & Dworetsky 1993) are the most obvious anomalies. Modern research shows that HgMn stars actually exhibit what appears to be a steady increase of overabundance with increasing atomic number (Ghazaryan & Alecian 2016). Other elements that can be readily confirmed as overabundant using ground-based data include P, Ga, Y, Xe, Pt, and Au. At the same time, light elements such as He are typically found to be underabundant (e.g., Castelli & Hubrig 2004). Strong isotopic anomalies have been detected for the chemical elements Ca, Pt, and Hg, with the patterns changing from one star to the next (Hubrig et al. 1999; Castelli & Hubrig 2004).

⋆ E-mail: drewski@nmsu.edu

Classification of HgMn stars based solely on the presence of Hg II and Mn II lines in the optical has naturally resulted in a very narrowly-defined and homogeneous sample compared to other chemically peculiar stars like the magnetic Ap/Bp stars and the (also poorly understood) metallic-lined Am/Fm stars. The HgMn stars cover a small spectral type range of B7–A0 main sequence stars (Renson & Manfroid 2009), and with an average rotational velocity of just $<v \sin i> \approx 30\,\mathrm{km\,s^{-1}}$ (maximum $v \sin i$ around $100\,\mathrm{km\,s^{-1}}$), they are slow rotators as a rule. Considering the HgMn star catalogs of Schneider (1981), Renson & Manfroid (2009), and Ghazaryan & Alecian (2016), as well as more recent finds by Alecian, et al. (2009); González & Levato (2009); Monier, Gebran & Royer (2015, 2016); Monier, et al. (2017); Ćalıskan & Ünal (2017); Hümmerich, et al. (2018), we estimate that there were 194 Galactic HgMn stars known prior to this work.

Over the past few decades it has become clear that the distributions of most or all elements on the surfaces of HgMn stars are inhomogeneous, i.e. these are **stars with chemical/abundance spots**. This was initially suspected by Hubrig & Mathys (1995) based on the dramatically differing strength of the Hg II 3984 Å line for binary HgMn stars with similar spectral types but different inclination angles, and it was confirmed for the first time by Malanushenko (1996), who found that the radial velocities of the He I lines of α And were variable with a period corresponding to the rotation period of the star. Recent high-resolution spectroscopic studies have subsequently shown that abundance spots on HgMn stars are the rule rather than the exception (Briquet, et al. 2010; Hubrig, et al. 2010; Makaganiuk, et al. 2011, 2012, etc.). The spot patterns not only differ strongly from element to element, they are also highly variable, changing over timescales as short as a few months (e.g., Korhonen, et al. 2013). It **is** well known that in the case of Ap/Bp stars, the **spot** patterns are correlated with the topology of their strong, global magnetic fields. The existence of abundance spots on the comparatively non-magnetic HgMn stars is therefore quite perplexing. However, the problem may be partially resolved by the recent detection of variable, weak, tangled magnetic fields in a small sample of HgMn stars (Hubrig et al. 2020, submitted).

Another key aspect of HgMn stars seems to be their high rate of binarity/multiplicity. Based on a check of literature radial velocity and binary orbit studies, Hubrig & Mathys (1995) found that the multiplicity fraction may be as high as 67% and that there was a preference for orbital periods shorter than 20 days. Schöller, et al. (2010) subsequently used high-contrast imaging to detect visual companions around 28 of 56 observed HgMn stars, suggesting a multiplicity fraction of at least 50%. Recently, Kervella, et al. (2019) studied the multiplicity fraction of nearby stars by combining proper motions from the Hipparcos and Gaia catalogs to check for proper motion anomalies (PMa) indicative of one or more companion objects. Of the 155 HgMn stars included in the study, 60/155 are known visual multiple stars and 36 of these 60 exhibit significant PMa. Another 43 HgMn stars for which companions have not been visually identified also exhibit signficant PMa, leading to a total of 103/155 (66%) definite or possible multiples, consistent with the findings of Hubrig & Mathys (1995).

The companions of HgMn stars are frequently also found to be chemically peculiar. The bright HgMn binary 46 Dra is one of the more remarkable examples, since the companion is a nearly equal mass star that also shows the HgMn pecularities (Tsymbal, et al. 1998). The 41 Eri, HR 7694, and HD 33647 systems are further examples of HgMn+HgMn binaries. A few systems also include magnetic chemically peculiar companions, with fields having been measured in the Am companion of χ Lup (Mathys & Hubrig 1995) and in the Ap companion of HD 161701 (Hubrig, et al. 2014). The latter system is noteworthy in terms of being the only known example of an HgMn+Ap binary (González, et al. 2014). More typically, the companions are found to be Am stars, especially the cooler ones (Ryabchikova 1998).

In the HgMn binaries with synchronously rotating components, the stellar surfaces facing the companion star usually display low-abundance element spots, whereas the surface of the opposite hemisphere, as a rule, is covered by high-abundance element spots (Hubrig et al. 2012). Membership in binary and multiple systems may therefore be an important clue toward developing a better understanding of HgMn stars.

The puzzling pattern of chemical abundances and variability, as well as the poorly understood role of magnetic fields in the HgMn stars challenges our very understanding of the nature of these objects. In the following, we report on the detection of 269 HgMn stars (only 9 previously known) in the H-band spectra obtained within the framework of the SDSS/APOGEE survey. This new sample represents a more than doubling of the number of known HgMn stars, and is generally an extension of the known sample to fainter magnitudes than have been probed in past studies. In addition to analyzing the H-band line content and line profiles of HgMn stars for the first time, we use the multi-epoch spectra available for most of the stars to measure radial velocities (RVs) and search for binaries. Where possible, we also estimate orbital parameters for the numerous single-lined (SB1), double-lined (SB2), and triple-lined (SB3) spectroscopic binaries among the sample.

2 DATA

2.1 SDSS/APOGEE H-band Spectroscopy

The APOGEE instruments are 300-fiber, $R = 22{,}500$, H-band spectrographs that operate on the Sloan 2.5m telescope (Gunn, et al. 2006) at Apache Point Observatory (APO, APOGEE-N) and on the Du Pont 2.5m telescope (Bowen & Vaughan 1973) at Las Campanas Observatory (LCO, APOGEE-S). Each APOGEE instrument records most of the H-band (15145–16960 Å; vacuum wavelengths used in this paper) on three detectors, with coverage gaps between 15800–15860 Å and 16430–16480 Å (Wilson, et al. 2019) and with each fiber subtending a $\sim 2''$diameter on-sky field of view. The typical exposure time for an APOGEE 'field' (1.5°–3° diameter area of sky) is one hour, or roughly the time needed to reach signal-to-noise ratios (S/N) of 100 for stars with $H \leqslant 11$ mag. The fields are usually observed multiple times on different nights, months, or years, to accumulate signal for fainter targets, and the individual spectra are later combined to produce high quality spectra for chemical abundance analysis. Majewski, et al. (2017) provided a

detailed overview of the APOGEE survey, and Nidever, et al. (2015) described the data reduction process. This paper makes use of spectra obtained during both SDSS-III (Eisenstein, et al. 2011) and SDSS-IV (Blanton, et al. 2017) and reduced by the 15$^{\rm th}$ SDSS data release (DR15; Aguado, et al. 2019) version of the reduction pipeline.

The APOGEE targeting strategy was summarized by Zasowski, et al. (2013, 2017), but some of the relevant details will be repeated here. In each APOGEE observation, 15–35 telluric standard stars (*TSS*) are targeted to facilitate removal of telluric absorption features from the science spectra. The *TSS* are selected quasi-randomly based on raw (undereddened) Two Micron All-Sky Survey (2MASS; Skrutskie, et al. 2006) $J-K$ color within an H-band magnitude range of $7.0 < H < 11.0$. There are also spatial restrictions to account for variability of the telluric absorption over the 2°–3° fields, and during SDSS-III, they were often excluded if positioned within the projected radius of an open cluster since this might induce collisions with the fiber casings of cluster science targets. In general however, the *TSS* are the combined bluest and brightest available stars in the field of view. As of July 8, 2019, a total of 33,838 *TSS* had been observed 192,545 times for an average of 5.7 spectra per star. The HgMn sample described here is culled primarily from the *TSS* sample, though with a few stars having been targeted as confirmed or candidate open cluster members during SDSS-IV. The HgMn sample at hand averages S/N=184 per individual spectrum, such that we are firmly operating in the high-S/N regime.

2.2 APO 3.5m + ARCES Optical Spectroscopy

We also obtained optical spectra of 32 newly discovered HgMn stars, 15 previously known HgMn stars, and Vega using the Astrophysical Research Consortium Echelle Spectrograph (ARCES; Wang, et al. 2003) on the ARC 3.5m telescope at APO. In each exposure, ARCES covers the full optical spectrum (3500–10400 Å) at a resolution of R=31,500. We used standard Image Reduction and Analysis Facility (IRAF[1]) echelle data reduction techniques, including 2D to 1D extraction, bias subtraction, scattered light and cosmic ray removal, flat-field correction, wavelength calibration via Thorium–Argon lamp exposures, as well as continuum normalization and merging of orders. The majority of the new HgMn stars were observed on multiple epochs in order to improve the derived orbital solutions. Exposure times were tailored to ensure S/N>100 at 4000 Å in each observation. A full log of the optical observations is provided in the appendix of this paper.

3 SAMPLE SELECTION

The HgMn star sample discussed in this paper was discovered among a much larger catalog of APOGEE Chemically Peculiar (ACP) stars that currently consists of >2100 stars collectively with ∼12,800 individual spectra. Assembly of the ACP catalog has been based primarily on detection of the Ce III lines at 15961, 15965, and 16133 Å (with weaker lines occasionally present at 15720 and 16293 Å), as described in Chojnowski, et al. (2019). These are often the strongest metallic features in the H-band spectra of Ap/Bp stars, and they are often the only metallic features present in the spectra of these stars. Roughly 26% of the ACP sample consists of stars that do not exhibit the Ce III lines and were instead added to the catalog due to prior classifications of chemical peculiarity in the literature.

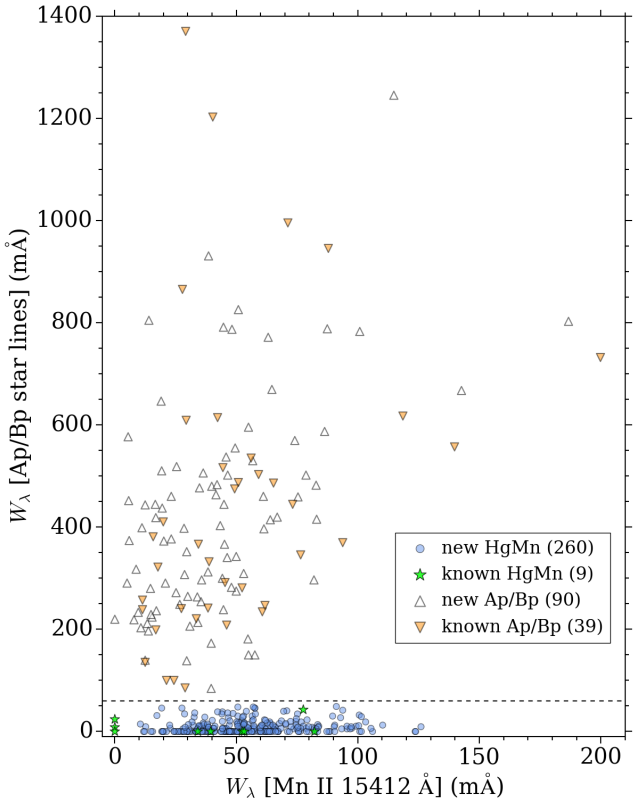

Figure 1. HgMn **versus** Ap/Bp classification, **based on comparison of the strength of lines that typically appear in Ap/Bp star spectra to the strength of Mn II 15413 Å.** The ordinate is the sum of the equivalent widths of Ce III 15961, 15965, Cr II 15370, 15470 Å, and the unidentified lines at 15231 and 16184 Å (discussed in Chojnowski, et al. 2019). We classify as HgMn any stars below the dashed line at $y = 60$ mÅ.

The Ce III lines are also useful for identifying Am/Fm stars despite the 'normal star lines' (*NSL*), i.e. the Mg I, Si I, Fe I, C I, S I, and Al I lines that are present in the APOGEE spectra of nearly all stars with effective temperature less than ∼8000 K, always being stronger than Ce III for Am/Fm stars. Both Ap/Bp and Am/Fm stars can exhibit the *NSL* however, such that there is some ambiguity. Based on inspection of the spectra of the many hundred stars in the ACP catalog with literature Ap/Bp or Am/Fm classifications, the two groups can be distinguished based on a quite simple criterion. Namely, the ratio of Ce III 15961 Å over the neighboring blend of Ce III 15964.928 Å + Si I 15964.424 Å is always less than unity for stars classified as Am/Fm, and vice versa for those classified as Ap/Bp stars. Another equally viable

[1] IRAF is distributed by the National Optical Astronomy Observatories, which are operated by the Association of Universities for Research in Astronomy, Inc., under cooperative agreement with the National Science Foundation.

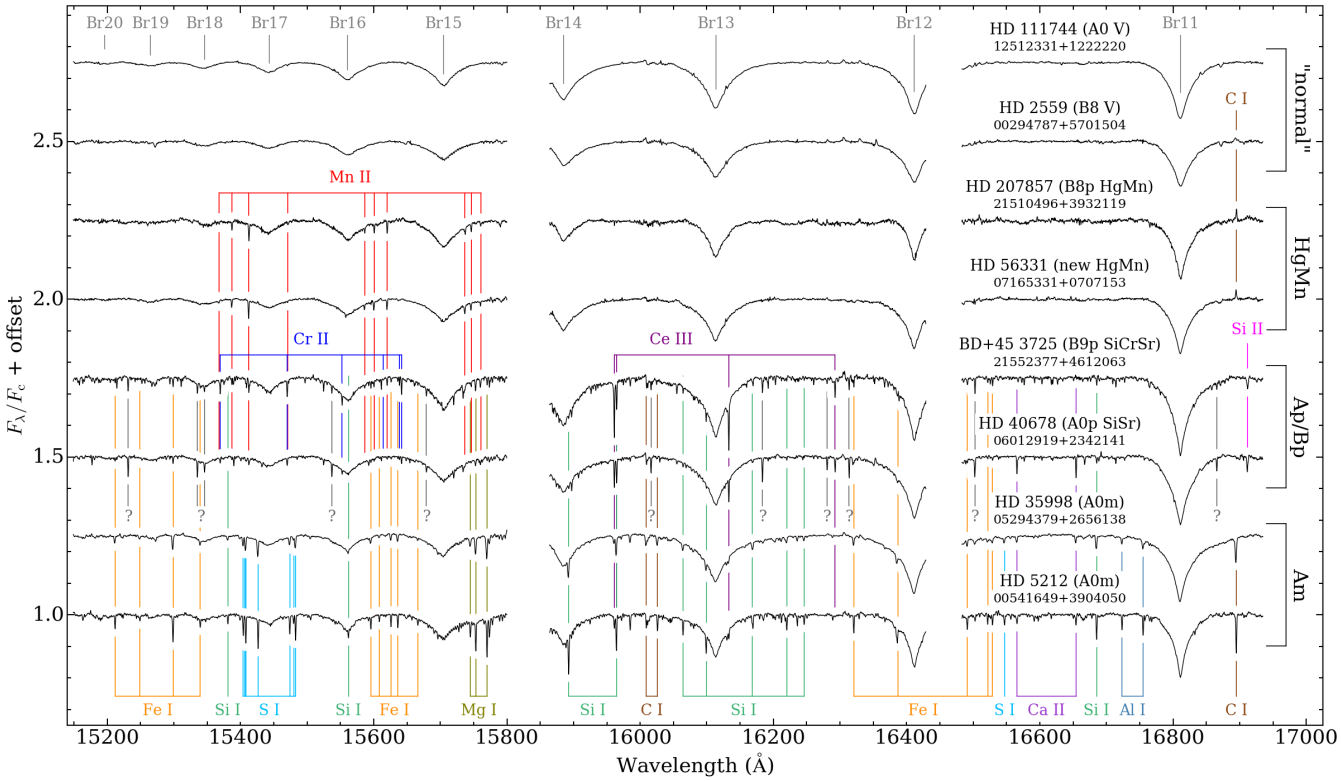

Figure 2. Comparison of the *H*-band spectra of new and previously-known HgMn stars (HD 207857 and HD 56331) to presumably normal stars (HD 2559 and HD 111744), Ap/Bp stars (BD+45 3725 and HD 40678), and Am stars (HD 35998 and HD 5212). Literature spectral types and 2MASS designations are given at right, and the majority of strong spectral features have been labeled. The line content of the normal stars is mostly limited to the hydrogen Brackett series lines, though HD 2559 exhibits weak emission in the C I 16895 Å line. The HgMn stars have strong Mn II and emission in C I 16895 Å. The Ap/Bp stars also have Mn II, but the strongest lines are from Ce III, Cr II, the unknown lines (labeled with question marks), Si II, and Ca II (in the case of HD 40678). The Am stars also exhibit Ce III, but the Mn II, Cr II, and unknown lines are never present. Instead, the 'normal star lines' (C I, Si I, S I, Mg I, Al I, and Fe I) are overly strong.

classification method is to check for the presence of lines that are only detected in the spectra of Ap/Bp-classified stars. Good options for this are the Cr II and Mn II lines, with perhaps the most useful option being the set of unidentified lines (*UL*) that are often prominent in Ap/Bp star spectra and that were used for magnetic field modulus measurement in Chojnowski, et al. (2019). Although we suspect the *UL* are formed by one or more rare earth elements, the associated atomic data do not exist or are not publicly available. Regardless, these lines do not appear in the spectra of Am/Fm stars.

One of the most severe outliers among the apparent **Ap/Bp** stars identified via Ce III detection was the well known HgMn star HD 207857, for which the metal absorption line content is limited to Mn II and Ce III, but with the strengths of the Mn II lines more than doubling those of the Ce III lines. This revelation prompted us to search the ∼40,000 APOGEE telluric standard stars for additional objects with Mn II absorption lines. This was done by measuring equivalent widths via direct integration of the flux contained in fixed 3 Å windows centered on the two strongest Mn II lines covered (15413 Å and 15620 Å). These lines conveniently fall in portions of the spectra that are unaffected by strong airglow emission or telluric absorption features. They are also well separated from any lines that might be expected to appear in the spectra of F-type or hotter stars, such that there is minimal confusion due to blending.

The search identified almost 500 stars with potential Mn II detections, and visual inspection of the resulting spectra confirmed ∼400 stars with Mn II. Five previously known HgMn stars (HD 36662, 45975, 49606, 158704, and 182308) were included, and unlike the case of HD 207857, the only metal lines in the associated spectra are Mn II (no Ce III). Furthermore, 44 stars recovered by the search are classified as classical Ap/Bp stars in the literature, and for 40 of these, the Mn II lines are accompanied by Ce III and either Cr II, the *UL*, or both. We therefore defined the HgMn sample based on comparison of the equivalent width of the strong Mn II 15413 Å line versus the sum of equivalent widths of Ce III 15961 and 15965 Å, Cr II 15370 and 15470 Å, and the *UL* at 15231 and 16184 Å. This comparison is shown in the Figure 1, with the dashed line at $y = 60$ mÅ indicating the fairly clean separation between HgMn stars and Ap/Bp stars.

The three star symbols in the extreme lower left corner of Figure 1 correspond to stars with literature Mn-peculiar classifications that did not produce the *H*-band Mn II lines in the available spectra. For Renson 3040 (A0 HgMn), the metal line content is limited to C I and Mg I, which is typical of mid–early A-type stars. For HD 51688 (B8 SiMn),

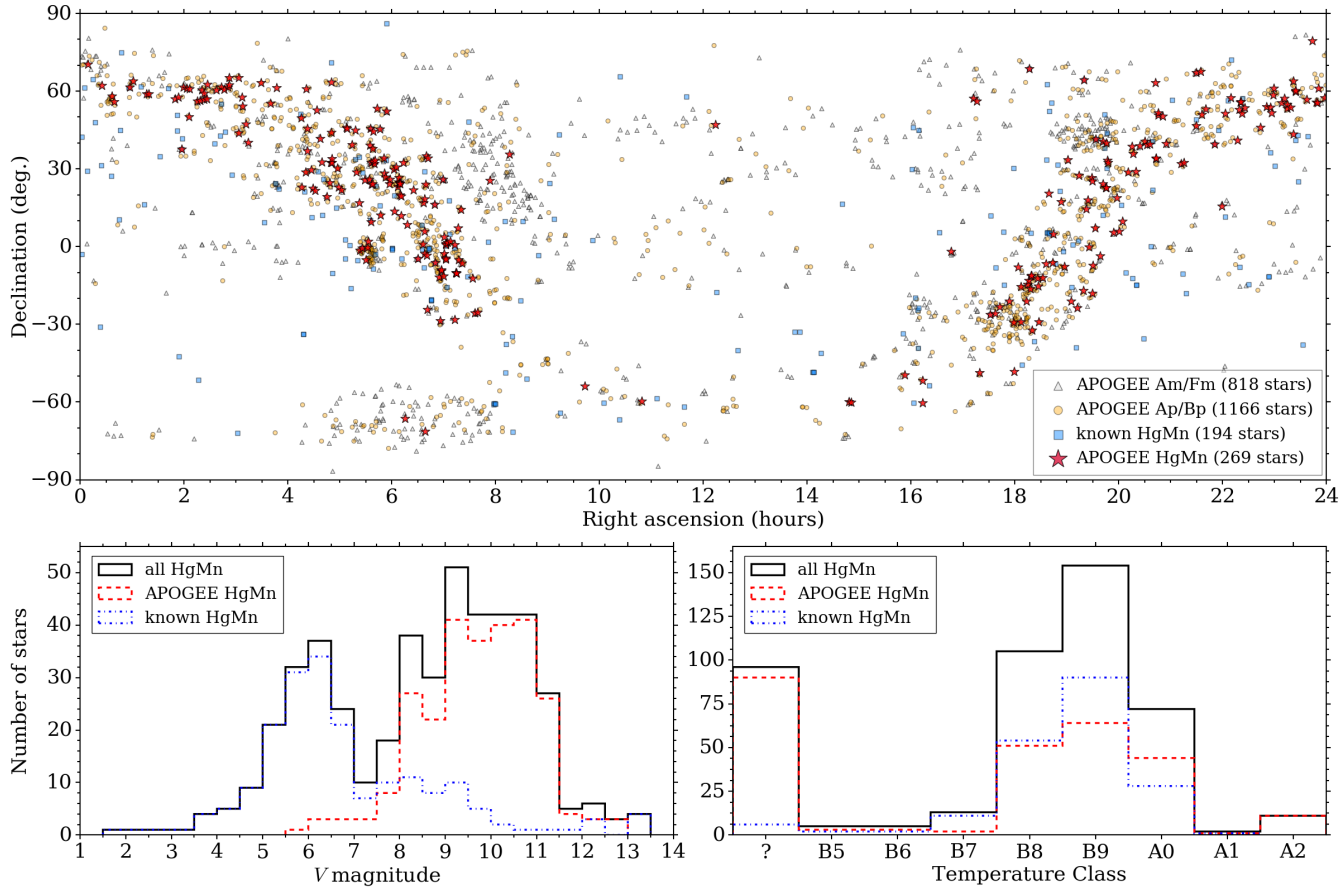

Figure 3. (*Top:*) Spatial distributions of the APOGEE chemically peculiar stars and the previously known HgMn stars. (*Lower left:*) Histogram of V magnitude for the HgMn stars. (*Lower right:*) Histogram of literature spectral types for the HgMn stars. The column labeled "?" in the lower right panel indicates the almost 100 HgMn stars that lack a literature spectral type.

Table 1. APOGEE HgMn Stars

2MASS Designation	Other Name	2MASS H (mag)	<S/N>	$N_{RV}/N_{obs.}$	$v \sin i$ (km s^{-1})	<W_λ> Mn II 15413 (mÅ)	<W_λ> Ce III 15961 (mÅ)	<W_λ> C I 16895 (mÅ)	<RV> (km s^{-1})	$RV_{scat.}$ (km s^{-1})	Binary Type	Literature Spectral Type
00091817+7022314	...	8.953	216	12/12	17 ± 8	35	...	-33	-19.1 ± 2.1	4.7	...	...
00245787+6212255	...	10.479	112	11/12	4 ± 4	23	...	-37	-29.5 ± 2.8	7.0	SB1	...
00364423+5810121	...	10.345	109	8/13	62 ± 2*	61	...	...	-31.5 ± 7.5	21.9	...	...
00390709+5558188	...	10.472	109	6/6	36 ± 7	54	...	...	-21.5 ± 5.4	2.6	...	...
00570626+6134007	HD 5429	8.403	268	11/11	20 ± 2*	30	...	-47	-3.2 ± 2.2	62.5	SB2*	B8 III[1]
01011057+6355294	Hilt 91	9.860	140	3/3	10 ± 4	82	...	-30	-27.7 ± 1.6	0.1	...	B9 III:[1]
01165086+5902504	...	9.709	129	4/4	58 ± 5	62	...	...	-15.5 ± 7.4	7.8	...	B8[1]
01191843+5902478	HD 7844	8.317	261	6/6	39 ± 2*	79	...	-72	-29.1 ± 2.0	4.3	...	B8[1]
01494647+5653549	...	10.600	88	3/3	15 ± 5	33	...	...	-31.8 ± 6.3	5.7	...	...
01533081+5736078	...	10.507	103	3/3	37 ± 8	56	13	...	-52.9 ± 6.4	6.7	...	...

[1] SIMBAD
[2] Renson 2009

no metal lines are present in the spectra. For HD 169027 (A0 Mn), Ce III 15961 Å and Si II 16911 Å are possibly present in lieu of the Mn II lines.

The distinctions between HgMn stars versus apparently normal stars, Ap/Bp stars, and Am/Fm stars are further emphasized in Figure 2, which displays APOGEE spectra of two examples each of apparently normal stars, HgMn stars, Ap/Bp stars, and Am stars. HgMn stars are most similar to the Ap/Bp stars in terms of line content, but only for the HgMn stars is the line content limited to Mn II with occasional Ce III absorption and C I emission. **We are not aware of any** examples of Ap/Bp stars with C I in emission,

Table 2. Atomic data for lines detected in the APOGEE spectra of HgMn stars. The Mn II, C I, and hydrogen (Brackett series) data are from the Kurucz line list. The Ce III data are from the Dream database.

Ion	$\lambda_{vac.}$ (Å)	$\log[gf]$	E_{lo} (eV)	E_{hi} (eV)	W_λ / W_{15413}
Mn II	15368.065	-1.002	9.863	10.670	0.19
Mn II	15387.220	-0.272	9.864	10.670	0.51
Mn II	15412.667	0.237	9.865	10.670	1.00
Mn II	15470.870	-1.869	9.007	9.809	0.12
Mn II	15586.570	-0.558	9.862	10.658	0.30
Mn II	15600.576	-0.140	9.863	10.658	0.52
Mn II	15620.314	-0.031	9.864	10.658	0.70
Mn II	15737.053	-0.303	9.862	10.650	0.50
Mn II	15746.494	-0.257	9.862	10.650	0.50
Mn II	15760.789	-0.479	9.863	10.650	0.34
Ce III	15961.157	-1.120	0.000	0.777	...
Ce III	15964.928	-1.660	0.815	1.591	...
Ce III	16133.170	-0.920	0.388	1.156	...
C I	16895.031	0.568	9.003	9.736	...
H-Br20	15196.005	-1.489	12.749	13.564	....
H-Br19	15264.717	-1.416	12.749	13.564	....
H-Br18	15345.991	-1.339	12.749	13.564	....
H-Br17	15443.148	-1.256	12.749	13.564	....
H-Br16	15560.708	-1.167	12.749	13.564	....
H-Br15	15704.960	-1.071	12.749	13.564	....
H-Br14	15884.888	-0.966	12.749	13.564	....
H-Br13	16113.721	-0.852	12.749	13.564	....
H-Br12	16411.681	-0.725	12.749	13.564	....
H-Br11	16811.117	-0.582	12.749	13.564	....

but as will be discussed in Section 7, it **is** a common trait of HgMn stars and exotic emission line stars. The spectrum of HD 2559 in Figure 2 demonstrates that the C I 16895 Å line is also occasionally in emission for superficially normal late-B and early-A stars.

3.1 Sample Parameters

Figure 3 **presents** some basic parameters of the sample, including the spatial, brightness, and temperature classification distributions. As expected, the vast majority of APOGEE HgMn stars are located near the Galactic midplane, having been observed in the grid of relatively-high-extinction Disk fields that have been the primary focus of the APOGEE survey. The sparsity of stars below declination $\simeq -30°$ is caused by several factors, not **only** limited to the later start date of APOGEE-2 observations on the Du Pont Telescope. Another factor is the fact that during APOGEE-1 and part of APOGEE-2N, 35 telluric standard stars were observed per field. Partway into APOGEE-2 however, it was decided that the telluric correction would not suffer if that number was decreased to 15. Therefore, only 15 telluric standard stars per field have been observed during some of APOGEE-2N and all of APOGEE-2S. Further, the on-sky radii of the plug-plates for APOGEE-2S are typically 0.8°, as compared to the 1.5° on-sky radii of APOGEE-2N plug-plates. The reduced field-of-view often leads to cooler stars being selected as telluric standard stars.

As demonstrated in the lower left panel of Figure 3, the APOGEE sample of HgMn stars is essentially an extension of the known sample to fainter magnitudes. The combined V magnitude distributions of known versus new HgMn stars suggest that many more examples should exist between $7 < V < 8$. Although a large fraction of the APOGEE HgMn sample lacks any indication of spectral type in the literature, the lower right panel of Figure 3 shows that the available spectral types are in line with expectations set by the previously known sample. With limited exceptions, the HgMn stars cover a remarkably narrow spectral type range of B7–A0.

The APOGEE HgMn star sample is summarized in Table 1, which provides for each star the 2MASS designation, an alternative identifier, the 2MASS H magnitude, the average S/N, the number of radial velocity (RV) measurements compared to the overall number of spectra, $v \sin i$, the average equivalent widths (W_λ) of Mn II 15413 Å, Ce III 15961 Å, and C I 16895 Å, the average RV, the maximum difference between individual RVs ($RV_{scat.}$), an indication of binarity, and if it exists, a literature spectral type from either SIMBAD or the chemically peculiar star catalog of Renson & Manfroid (2009).

In the Binary Type column of Table 1, "VIS" indicates that the star is known visual double or multiple system, "SB1 (lit.)" indicates the star has been reported as a binary in the literature, and asterisks indicate that an orbital solution is reported in this paper (see Section 6.1). Asterisks next to the $v \sin i$ values in Table 1 indicate that $v \sin i$ was derived from optical spectra.

3.2 *H*-band Linelist

Atomic data for lines that can appear in the H-band spectra of HgMn stars are given in Table 2. The Kurucz linelist[2] includes 145 Mn II lines, but only the **strong lines (in terms of $\log_{10}$ of the product of statistical weight, g, and oscillator strength, f)** with lower energy levels around 10 eV are detected. Although there are no Hg lines in the H-band, all of the new HgMn stars we observed in the optical exhibit Hg II, such that **it** is safe to say that a star whose H-band line content is limited to Mn II is almost certainly a bona fide HgMn star. The W_λ / W_{15413} column of Table 2 gives the average equivalent width ratios of the Mn II lines over Mn II 15413 Å, based on measurements of the lines in spectra of stars with exceptionally strong Mn II. See Chojnowski, et al. (2019) for a list of the empirical rest wavelengths of the *UL*.

3.3 Optical Verification

Figures 4 and 5 display selected regions of the optical follow-up spectra for new and previously known HgMn stars, allowing us to verify that the new finds are indeed HgMn stars as defined in the optical. Detection of He I lines at strengths less than that of Mg II 4481 Å indicates that all of the stars fall in the B7–A0 temperature class range, as expected for HgMn stars. With the exceptions of HD 211838 and Maia, the Hg peculiarity is confirmed for all of the stars via detection of Hg II 3984 Å, which is typically the strongest Hg II line in the optical spectra of HgMn stars (Cowley & Aikman 1975). Depending on rotational velocity, dozens to hundreds of Mn II lines are readily identified in the spectra

[2] http://kurucz.harvard.edu/lineslists/

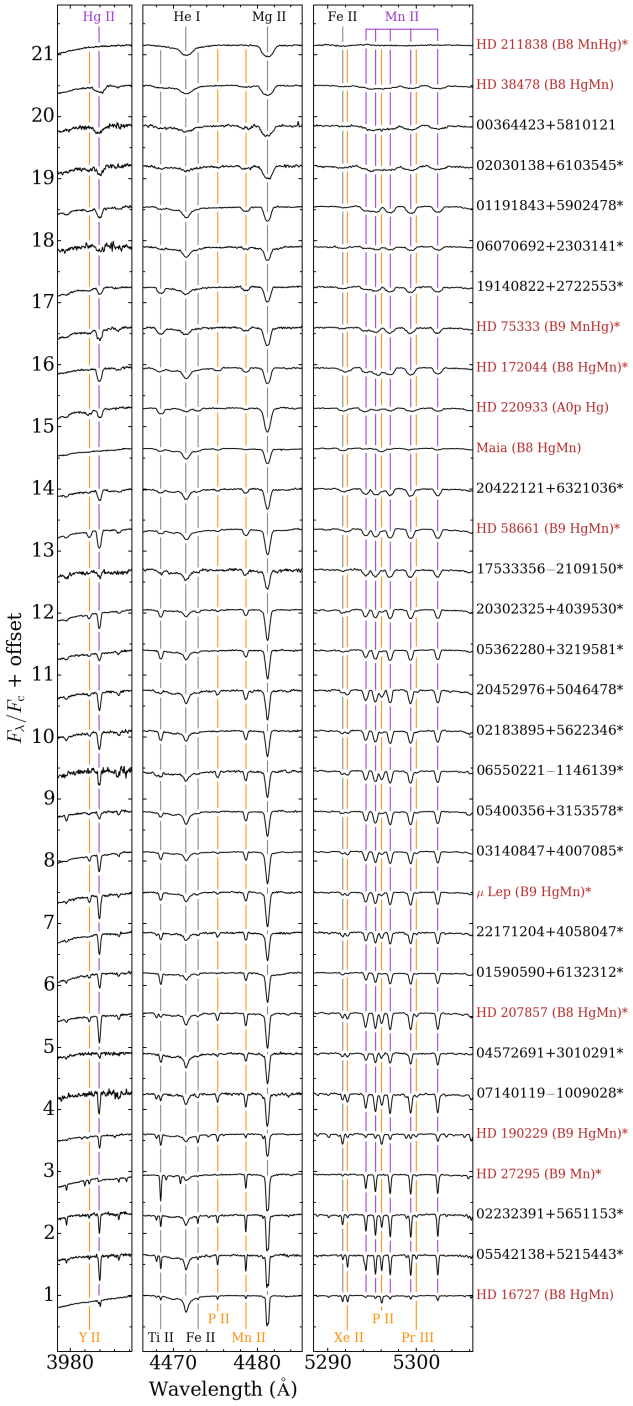

Figure 4. Optical spectra of SB1 and apparently single HgMn stars, showing regions centered on Hg II 3984 Å, He I 4471 Å and Mg II 4481 Å, and the Mn II lines between 5294–5302 Å. The spectra are sorted vertically by $v \sin i$, going from 66 km s^{-1} for HD 211838 down to 2.8 km s^{-1} for HD 16727. Star names and 2MASS designations are given for the known and new HgMn stars, respectively, with literature spectral types given for the known HgMn stars and with asterisks indicating stars that are definite or suspected binaries. Grey vertical lines indicate features that appear in the spectra of normal B7–A0 stars, while purple and orange vertical lines indicate features that only appear in the spectra of chemically peculiar stars.

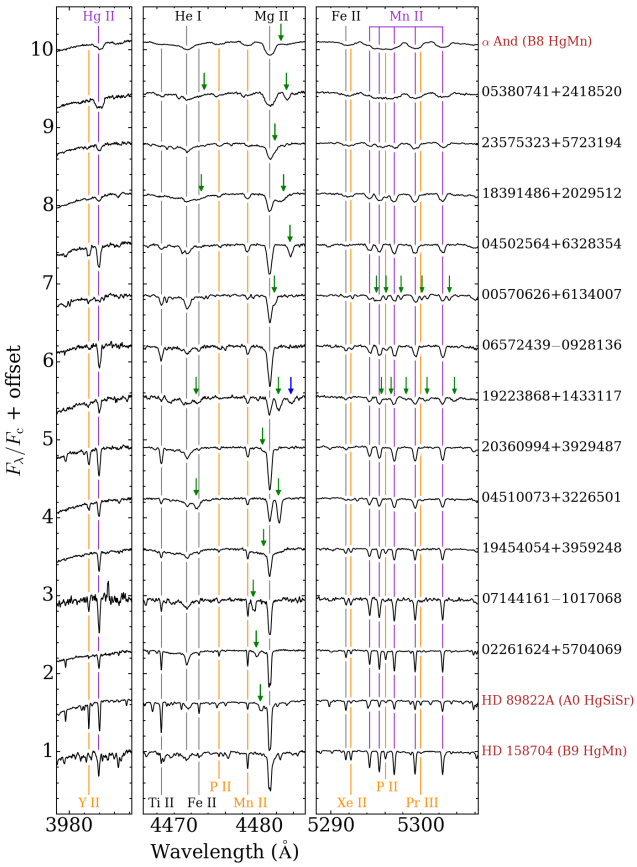

Figure 5. The same as Figure 4 but for binary systems identified as multi-lined in either the optical or *H*-band. **Small green arrows mark lines from the secondary stars in cases of > 20 km s^{-1} velocity separations of the components, and in the case of the SB3 2MASS J19223868+1433117, a blue arrow marks the Mg ii 4481 Å line of the tertiary star.**

of the new HgMn stars, thus confirming the Mn peculiarity. The atlas of Castelli & Hubrig (2004) was particularly useful for identifying weak heavy metal features, and indeed many of the stars exhibit anomalously strong lines from P II, Ga II, Y II, Zr II, Xe II, Pt II, Pr III, and Nd III, all of which are known to be overabundant in HgMn stars (Ghazaryan & Alecian 2016). The stars 2MASS J02232391+5651153 and 2MASS J05542138+5215443 (near the bottom of Figure 4) are perhaps the most extreme HgMn stars of our optical sample. We were able to identify ∼300 Mn II lines in the optical spectra of both stars, along with 83 P II lines and 13 Xe II lines in the spectrum of 2MASS J05542138+5215443.

The only stars represented in Figures 4 and 5 for which no evidence of binarity or multiplicity has been either reported in the literature or in this paper are HD 38478, 2MASS J00364423+5810121, HD 220933, and Maia. All of the new HgMn stars were targeted for optical follow-up due to being likely or definite SB1s and SB2s. For most of the stars represented in Figure 5, blue arrows mark the positions of the binary companions' Mg II 4481 Å lines and occasionally also of the companions' He I 4471 Å lines. For 2MASS J06572439−0928136 and HD 158704, the companions are separated from the primaries by < 20 km s^{-1}, such

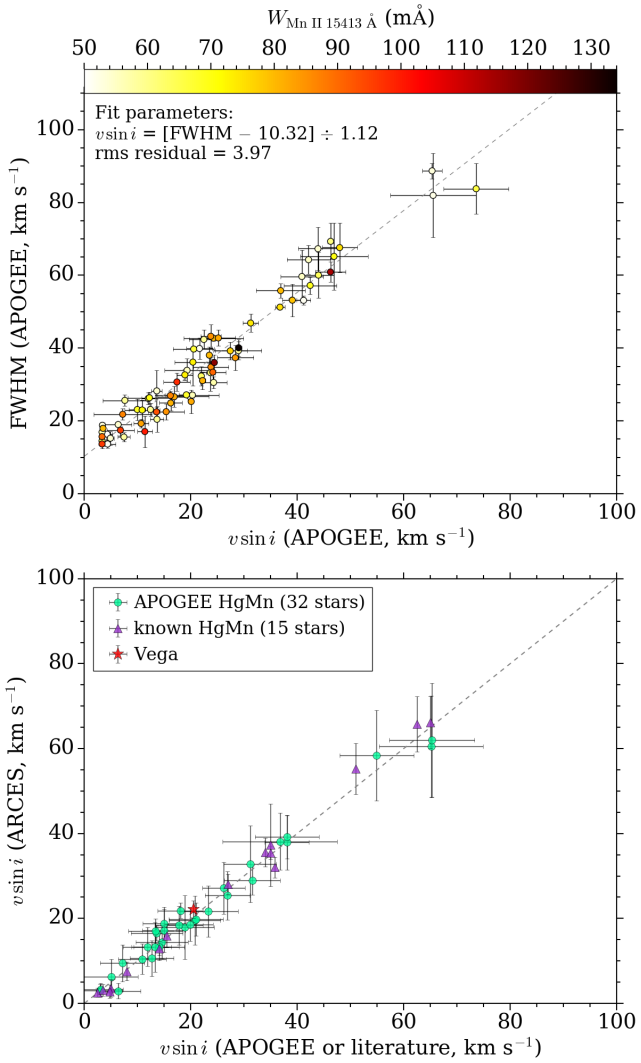

Figure 6. (*Top:*) A linear fit to the relation between **goodness-of-fit $v \sin i$ results from the *iacob broad* code versus Gaussian FWHMs of the same lines**. Both quantities are the averages of multiple Mn II lines, and the points are colored by the equivalent width of Mn II 15413 Å. (*Bottom:*) **A comparison of $v \sin i$ measured from our optical spectra versus $v \sin i$ from the *H*-band data or the literature**, with a dotted line at $y = x$. For the previously-known-but-not-observed-by-APOGEE-stars (purple triangles), the **abscissa** gives a literature $v \sin i$ estimate.

that the companion contributions to strong lines are thoroughly blended with the primary star lines. For α And, the companion is difficult to detect owing to the rapid rotation of both stars, so the arrows simply mark the expected companion position based on the orbit presented by Ryabchikova, Malanushenko & Adelman (1999). In the cases of the SB2 2MASS J00570626+6134007 and the SB3 2MASS J19223868+1433117, the primary and secondary stars both produce optical Mn II lines. The Mg II 4481 Å line of the tertiary in the latter system is marked with a blue arrow in Figure 5. Most of these stars will be discussed in more detail in Section 6.

4 RADIAL VELOCITIES

Having established the HgMn sample, we proceeded to use the *H*-band Mn II lines to measure RVs by interactively fitting Gaussians to as many Mn II lines as possible from 1584/1709 APOGEE spectra (excluding some low S/N data) using the *splot* program of IRAF. From this we obtained estimates of the line centers, FWHMs, and W_λ. The line position measurements from each spectrum were averaged and a barycentric correction was added to produce the heliocentric RVs quoted in this paper. For the errors, we simply adopted the standard deviation (σ) of the line-by-line measurements. In most cases, at least two Mn II lines (usually 15413 Å and 15620 Å) were resolved in each spectrum, but in spectra where only the strongest Mn II line (15413 Å) was resolved, we assign a constant RV error of 10 km s^{-1}.

For the optical follow-up sample, the same process described above was applied to numerous Fe II, Si II, Cr II, Ti II, Mn II, and O I lines. The epoch-by-epoch RV measurements are provided in the appendix of this paper.

5 ROTATIONAL VELOCITIES

Rotational velocities ($v \sin i$) were estimated based on the Gaussian FWHMs measured for all of the stars and a calibration derived from a sub-sample of 71 stars with particularly strong *H*-band Mn II lines ($W_{\rm Mn\ II\ 15413} > 50$ mÅ) and high-S/N spectra. The latter analysis was carried out using the IDL code *iacob broad* (Simón-Díaz & Herrero 2014), which estimates $v \sin i$ via two methods: identification of the first zero of the Fourier transform of an observed line profile, and reduction of χ^2 via a goodness-of-fit (GOF) technique whereby a **theoretical line profile convolved with rotational and macroturbulent line-broadening components is compared to the observed line profile**. Due to considerably more scatter in a plot of the Gaussian FWHMs versus the Fourier transform $v \sin i$, we adopted the GOF $v \sin i$. The upper panel of Figure 6 shows the associated linear fit to the FWHM and GOF $v \sin i$.

The relation between $v \sin i$ and FWHM derived from the sub-sample of 71 stars was then used to convert the Gaussian FWHM measurements to $v \sin i$ for the stars with weaker and/or noisier line profiles. For error estimates, the FWHM standard deviations were added in quadrature to the root mean square residual of 3.97,km s^{-1} of the liner fit in the upper panel of Figure 6. From this, we find an average of $<v \sin i>$= 26.8 km s^{-1} for the APOGEE sample, which is quite close to the average $<v \sin i>$= 30.6 km s^{-1} for the previously known HgMn stars. The ranges of $v \sin i$ are also similar, going from 3–88 km s^{-1} for the APOGEE sample and 0–109 km s^{-1} for the known sample.

For the optical follow-up sample, we ran the *iacob broad* code on minimally-blended lines that are relatively strong in the spectra of all of the stars. This included lines of Fe II (4508, 4924, 5018, 5169 Å), Mn II (4479, 4756, 5559, 5571 Å), Si II (4128, 4131, 6347 Å), and O I (7772, 7774, 7775 Å). The average GOF $v \sin i$ results are plotted in the lower panel of Figure 6 against either the $v \sin i$ estimated from APOGEE spectra or else a literature value in the cases known HgMn stars which were not observed by APOGEE. The agreement is quite good, to within 5 km s^{-1} in most cases. Due to the

higher resolution and vastly greater number of available lines of the optical versus *H*-band spectra, Table 1 reports the $v \sin i$ measured from optical spectra for the optical follow-up sample.

6 MULTIPLICITY

HgMn stars are frequently or perhaps always member of binary or multiple star systems (e.g. Dolk, Wahlgren & Hubrig 2003; Schöller, et al. 2010), and the APOGEE sample is no different. This is demonstrated in the upper panel of Figure 7, which plots **the maximum difference between individual RVs ($\mathbf{RV_{scat}}$) versus $v \sin i$**. Since it is possible for chemical spotting to make the line centers vary over the course of a rotational period, leading to measurable RV variability, we conservatively classify as definite binaries or multiples the stars for which RV_{scat} exceeds $v \sin i$ **and/or the stars** that are clear SB2s. We also make **an exception** for 2MASS J05400356+3153578 since a convincing SB1 orbital solution was found. Although we did not find RV variability that exceeds $v \sin i$ for the previously known HgMn stars HD 45975 and HD 207857, long-period binarity has been reported by Andrews, Chanamé & Agüeros (2017) and Pourbaix, et al. (2004), respectively. These stars are represented by **square symbols** in Figure 7. The stars represented by **downward-facing triangle** symbols in Figure 7 are known visual doubles that we did not classify as binaries based on the APOGEE spectra.

In addition to the above SB1 classification criteria, we visually examined all available spectra to check for evidence of lines with RV offsets compared to the Mn II lines. A total of 19 SB2 systems were found based on the APOGEE data alone, including two systems that exhibit spectral lines from at least three stars (SB3s). Another four systems were confirmed as SB2s based on optical spectra, despite the companion stars not being detected in the APOGEE spectra.

Considering the 40 SB1 systems, 23 SB2s and SB3s, 11 visual double stars, and 2 previously known binaries, compared to the 165 stars whose RVs are not variable to within the projected $v \sin i$, we arrive at very conservative multiplicity fraction estimate of $N_{\rm multiples}/N_{\rm total} = 31\%$ (76 total multiples). However, due to the numerous stars for which the APOGEE observations were too few and/or over too short timescales for detecting anything but very short-period binaries, 31% is firmly a lower limit on the multiplicity fraction. As shown in the lower panel of Figure 7, the fraction increases toward longer observational baselines and/or more spectra, with for example the fraction being 18% for baselines shorter than 1.5 years and 44% for baselines longer than 1.5 years. Likewise, the multiplicity fraction is 19% for stars with five or fewer spectra, but it rises to 36% for stars with more than five spectra. Further observations of this sample will undoubtedly reveal numerous additional binaries/multiples, particularly those with long orbital periods.

It is important to note that the sample also includes several stars that we classify as possibly single despite many APOGEE spectra taken over relatively long timescales. The star 2MASS J19451699+2237253 (HD 344908, B8) is perhaps the best example, having been observed 38 times over a period of ~ 7.8 years. Compared to the majority of the sample, this star's Mn II lines are quite strong and narrow,

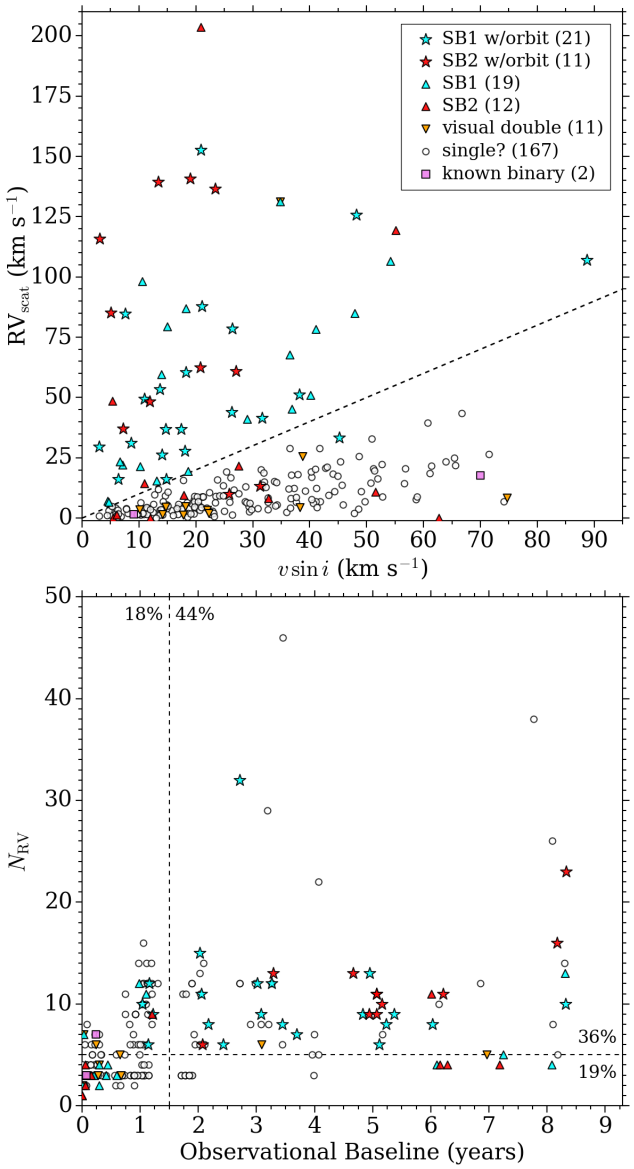

Figure 7. (*Top:*) Spectroscopic binary classification, whereby we consider everything with $\mathbf{RV_{scat} > v \sin i}$ **a definite binary or multiple, with a few exceptions. The dashed line indicates $\mathbf{RV_{scat} = v \sin i}$.** (*Bottom:*) Observational baseline versus number of RV measurements. The multiplicity fraction rises from 19% to 45% for stars with > 1.5 years observational baselines, and it rises from 20% to 37% for stars with more than five spectra.

such that there is minimal uncertainty about the RVs. The maximum RV difference between epochs for this star is just 3.7 km s^{-1}, implying that if a binary companion does exist, the orbital period is necessarily quite long or the companion mass quite low.

6.1 Binary Orbital Solutions

In the cases of RV-variable stars with at least six RV measurements, we attempted to determine Keplerian orbital parameters using the IDL code *rvfit* (Iglesias-Marzoa, López-Morales & Jesús Arévalo Morales 2015). This code utilizes

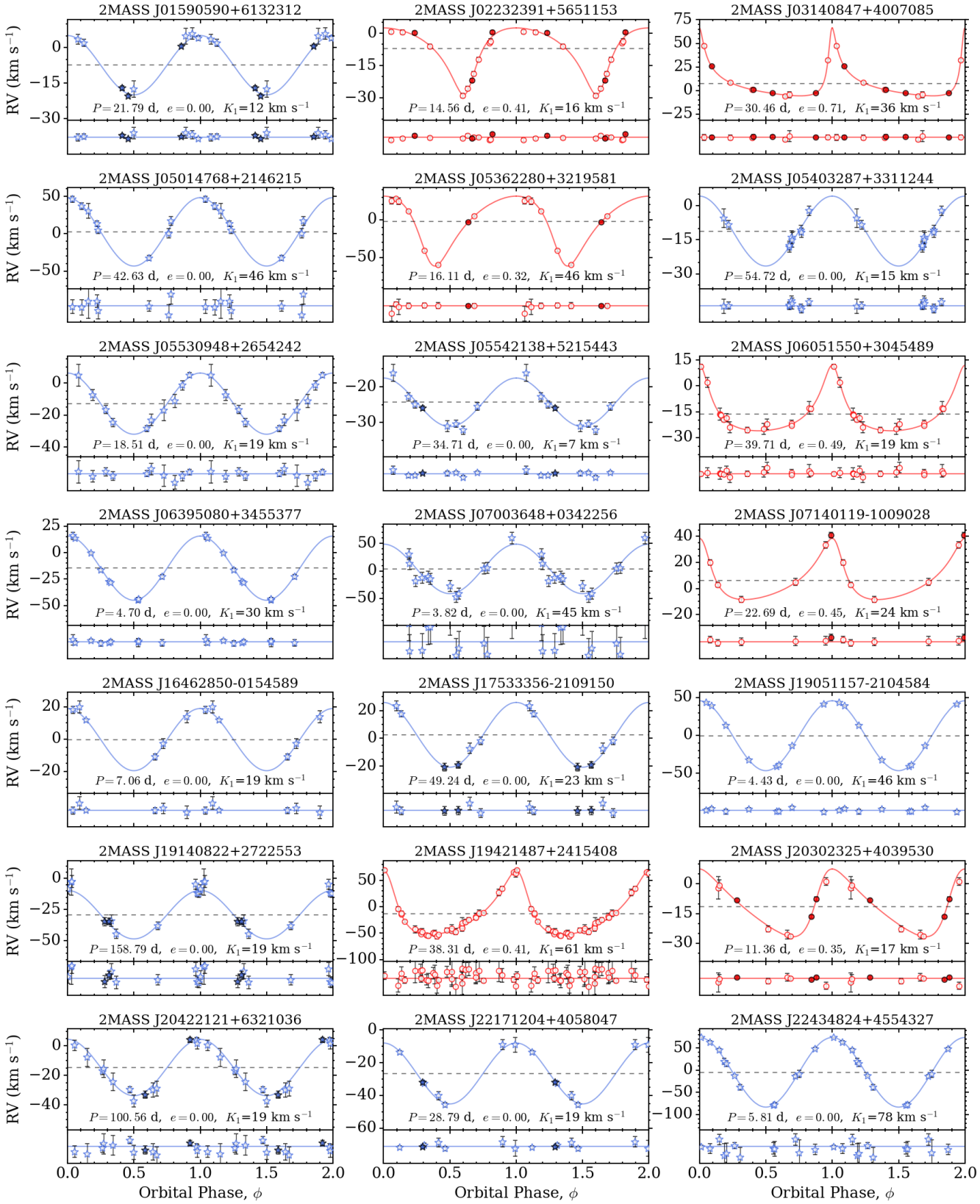

Figure 8. Orbital solutions for SB1s. The orbits have been repeated for two phases to improve the sense of continuity. Star symbols (blue) indicate **circular orbits, circle symbols (red) indicate eccentric orbits**, and filled symbols pertain to RV measurements from optical spectra. Dashed horizontal lines in the larger panels indicate the systemic velocities (γ), and solid lines are fits to the data. The smaller panels show the residuals of the observations minus the fit, with the ordinates covering $\pm 10\,\mathbf{km\,s^{-1}}$ and the horizontal lines indicating $y = 0$.

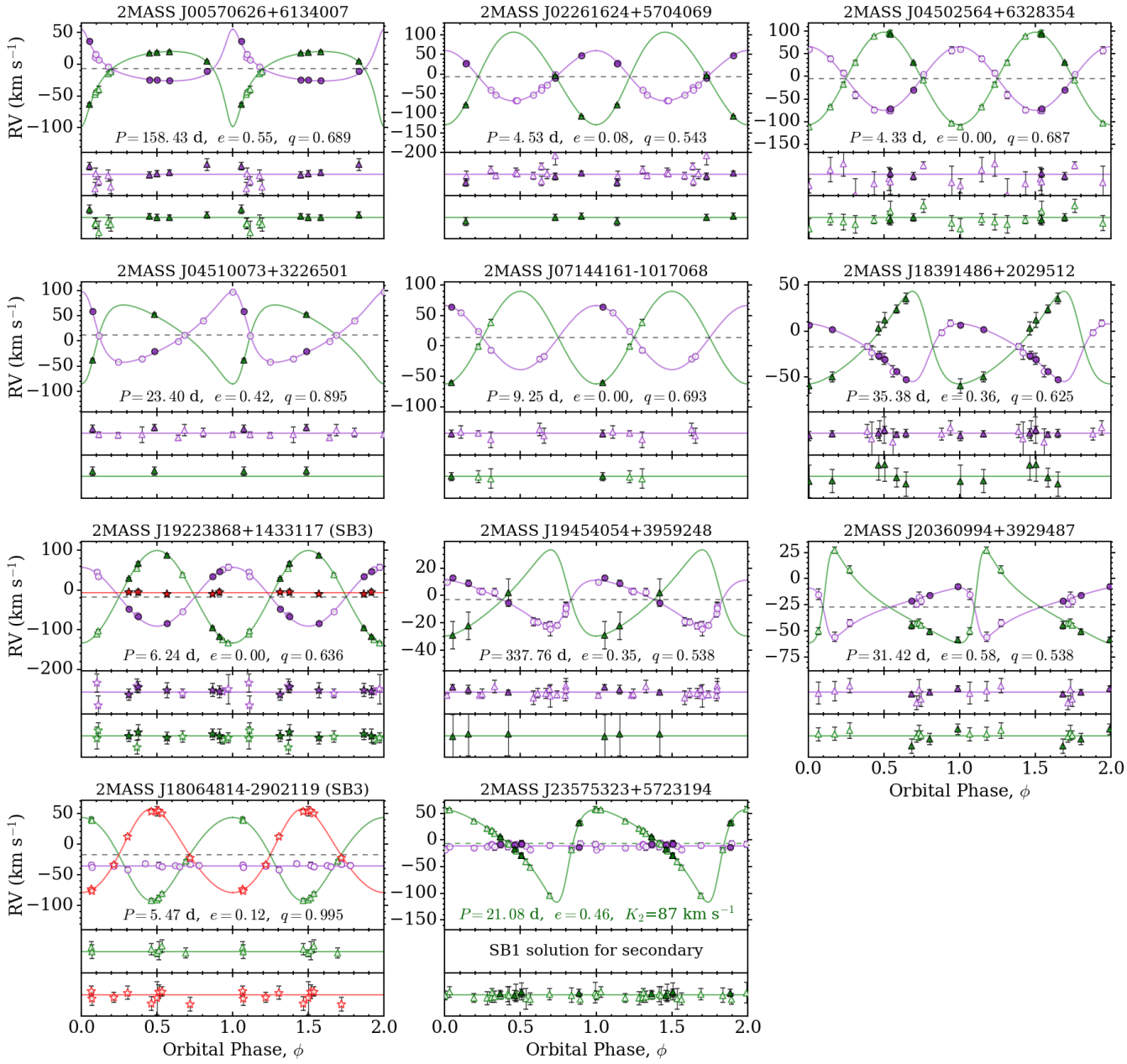

Figure 9. Orbital solutions for SB2s and multiple systems. Circle symbols (purple) are the RVs of the HgMn stars, triangle symbols (green) are the RVs of the secondary stars, star symbols (orange) are the RVs of the tertiary in the two SB3s, and filled symbols pertain to RV measurements from optical spectra. In the larger panels, dashed horizontal lines indicate the systemic velocity (γ), and if applicable, solid horizontal lines indicate the average RV of the binary component not included in the orbital solution. **The smaller panels are as described in Figure 8**. For the SB3 2MASS J18064814−2902119, an SB2 orbital solution pertaining to the secondary (Ap) and tertiary (A/Am) components is shown, while for the SB3 2MASS J19223868+1433117, an SB2 orbital solution pertaining to the primary (HgMn) and tertiary (Am) components is shown. For 2MASS J23575323+5723194, an SB1 orbital solution pertaining to the Am component is shown.

an Adaptive Simulated Annealing algorithm to determine orbital parameters for both SB1s and SB2s given inputs of heliocentric Julian dates (HJD), RVs, and RV errors. For SB1s, the code outputs seven parameters including the orbital period (P), time of periastron passage (T_P), orbital eccentricity (e), the argument of the periastron (ω), the systemic radial velocity (γ), the radial velocity semi-amplitude of the primary star (K_1). These parameters can then be used to determine the mass function ($f(m)$) and semi-major axis of the primary ($a_1 \sin i$). For SB2s, the radial velocity semi-amplitude of the secondary star (K_2) is another output, allowing for calculation of semi-major axes ($a_{1,2} \sin i$, $a \sin i$), dynamical masses ($M_{1,2} \sin i^3$), and the mass ratio ($q = M_2/M1$). Any of the output parameters from *rvfit* can be fixed to a particular value or constrained by upper and lower limits in an input configuration file. In all cases we

Table 3. Summary of double-lined and triple-lined spectroscopic binaries. Mass ratios ($q = M_2/M_1$) are given for the systems with orbital solutions, and flux ratios (F_2/F_1) of Mg II 4481 Å are given for the systems with optical spectra. The $v \sin i$ [1], $v \sin i$ [2], and $v \sin i$ [3] columns give rotational velocity estimates for the primary, secondary, and tertiary stars where applicable and where possible to make such estimates.

2MASS Designation	Companion Type(s)	Orbital Period (days)	Mass Ratio (M_2/M_1)	Mg II Ratio (F_2/F_1)	$v \sin i$ [1] (km s^{-1})	$v \sin i$ [2] (km s^{-1})	$v \sin i$ [3] (km s^{-1})	Note
09432220−5348264	HgMn	...	...	...	5± 5	5± 5	...	...
19223868+1433117	BpMn, Am	6.2	0.636	0.967, 0.438	18± 2	17± 2	22± 5	SB3; SB2 orbit for HgMn+Am components
00570626+6134007	Ap/Bp	158.4	0.689	0.245	20± 1	8± 2	...	...
02060290+5009136	Ap/Bp	...	...	...	34± 4	29±10	...	...
18064814−2902119	Ap/Bp, A/Am	...	...	...	26± 5	14± 6	15± 5	SB3; SB2 orbit for Ap+A/Am components
02261624+5704069	Am	4.5	0.543	0.203	3± 1	4± 1	...	companion not detected in APOGEE spectra
04502564+6328354	Am	4.3	0.687	0.352	22± 2	16± 3	...	...
05380741+2418520	Am	...	...	0.271	58± 3	15± 4	...	...
07144161−1017068	Am	9.3	0.694	0.328	6± 3	6± 3	...	...
17314436−2616112	Am	...	...	0.134	3± 1	13± 2	...	...
20360994+3929487	Am	31.4	0.536	0.115	13± 2	11± 3	...	...
23575323+5723194	Am	...	...	0.227	33± 2	11± 1	...	...
04510073+3226501	late-B	23.4	0.895	1.100	13± 2	10± 3	...	companion not detected in APOGEE spectra
18391486+2029512	late-B	35.4	0.625	0.787	25± 7	70±10	...	companion not detected in APOGEE spectra
19454054+3959248	late-B	337.8	0.538	∼1	9± 1	∼200	...	companion not detected in APOGEE spectra
02203397+6023494	A/Am	...	...	...	27±10	16± 7	...	multiple system?
04315476+2138086	A/Am	...	...	...	62± 8	62±15	...	...
06402199−0322092	A/Am	...	...	...	51± 9	23± 7	...	multiple system? Long-period SB2?
06561603−2839053	A/Am	...	...	...	9± 4	22± 5	...	...
06572439−0928136	A/Am	...	...	...	28± 4	15± 6	...	...
14482274−5959316	A/Am	...	...	...	21±11	18± 9	...	...
16133258−6019519	A/Am	...	...	...	11± 4	...	...	tentative detection in all APOGEE spectra
19294384−1801510	A/Am	...	...	...	12± 5	18± 7	...	...

began with very loose parameter constraints and with e as a free parameter, but in cases where the value of e became comparable to its error, we forced circular orbits by setting $e = 0$. Since T_P is undefined for circular orbits, we instead provide an epoch of maximum RV ($T_{\mathrm{max.RV}}$) regardless of e.

Orbital solutions for 21 SB1 systems and for at least one component in 11 SB2 and SB3 systems are presented in Figures 8 and 9, with open symbols pertaining to RVs measured from APOGEE spectra and filled symbols pertaining to RVs measured from optical spectra. The periods range from 4–338 days, with only six systems having periods longer than 50 days. Non-zero eccentricities are found in 15 cases, led by the $e = 0.72$ of the SB1 2MASS J03140847+4007085.

The minimum number of RV measurements for which we were able to find a reasonable orbital solution was six in the cases of the SB1s 2MASS J07140119−1009028, 2MASS J16462850-0154589, and 2MASS J17533356-2109150, and for the SB2 2MASS J07144161-1017068. Only for 2MASS J07144161-1017068 is the solution stable however, thanks to a group of five APOGEEspectra separated by just 63 days. For 2MASS J16462850-0154589, numerous periods between 6–60 days are just as reasonable as the result shown in Figure 8, and the orbit may also be slightly eccentric. For 2MASS J17533356-2109150, another common solution beyond the one shown in Figure 8 has $P = 171$ days. The orbits of these stars will likely be revised by additional observations.

The full orbital parameters of the SB systems presented in Figures 8 and 9 are provided in the appendix of this paper.

6.2 Binary Companions

The majority of the *H*-band-detected companions were evident in the *NSL* (namely, C I, Mg I, Si I, and occasionally S I), but not in the Ce III lines, indicating that they are either A or Am stars (see the Am star spectra in Figure 2). As these stars are significantly fainter than the HgMn primaries, the features are typically quite weak, often only becoming evident after smoothing the spectra. For Am stars, the Ce III lines are always significantly weaker than Mg I and Si I such that **we do not** expect to be able to distinguish a normal A-type companion from an Am companion in the APOGEE spectra of HgMn SB2s. The Ce III lines would likely be below our detection threshold. We therefore refer to the companions in these systems simply as "A/Am" due to the ambiguity, but in reality it would not be surprising if the majority of the companions were indeed chemically peculiar stars.

On the other hand, at least 11 of the SB2 systems definitely involve chemically peculiar companions. This includes four cases of Ce III lines that are offset from Mn II, if not clearly varying in anti-phase with respect to Mn II, and one case of multiple sets of Mn II lines in the APOGEE spectra. In another six cases, we classify the companions as Am stars based on detection of corresponding Sr II and Ba II lines in optical follow-up spectra (known to be overabundant for Am stars; see Ghazaryan, Alecian & Hakobyan 2018).

Table 3 summarizes the multi-lined systems, providing the companion types and $v \sin i$ along with the mass ratios for systems with orbital solutions, and Mg II 4481 Å flux ratios for systems with optical spectra. For systems with optical spectra in which the companion lines were sufficiently separated from the primary lines, the companion $v \sin i$ estimates were determined using the *iacob broad* code. Otherwise, the calibration presented in Figure 7 was used. In many cases, the binary components have nearly or definitely identical $v \sin i$, and in only three cases do we find one or more components with $v \sin i > 30$ km s^{-1}.

As noted in Section 6, the companion stars of four SB2s

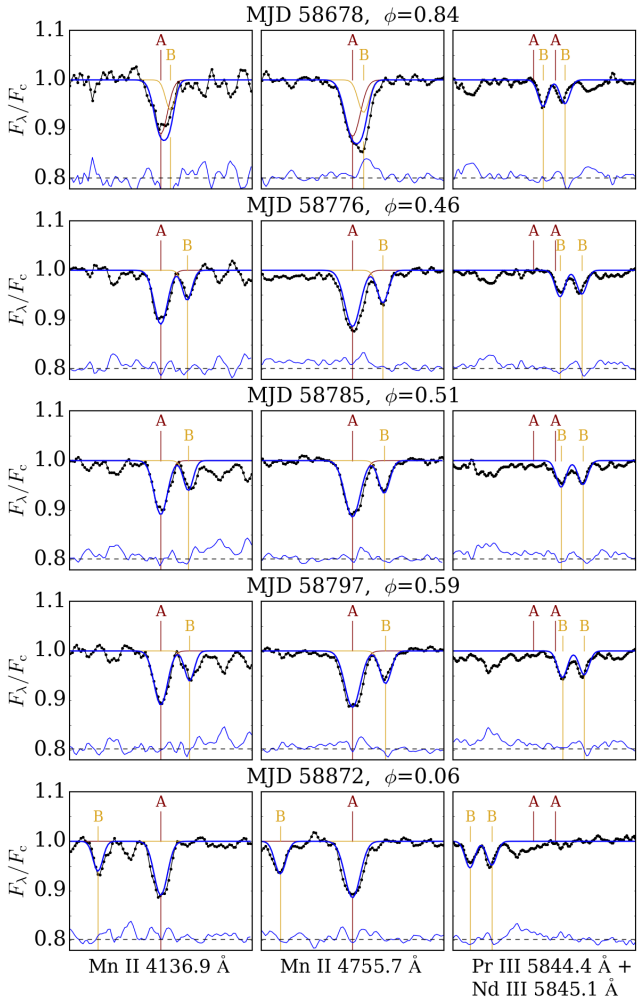

Figure 10. Optical spectra of the HgMn+Ap/Bp binary 2MASS J00570626+6134007 (HD 5429), highlighting the Mn II lines that are produced by both stars and the rare earth lines (e.g. Pr III and Nd III) that are produced by the Ap star (B) but not by the HgMn star (A). The spectra are shown in the rest frame of the HgMn star, and with individual Gaussians fits to the lines of each star (red and orange) as well as the sum of contributions from both stars (blue). Residuals are shown along the bottom of each panel, shifted upward artificially with the dashed lines indicating $y = 0$. The quoted orbital phases pertain to the orbital solution shown in Figure 9.

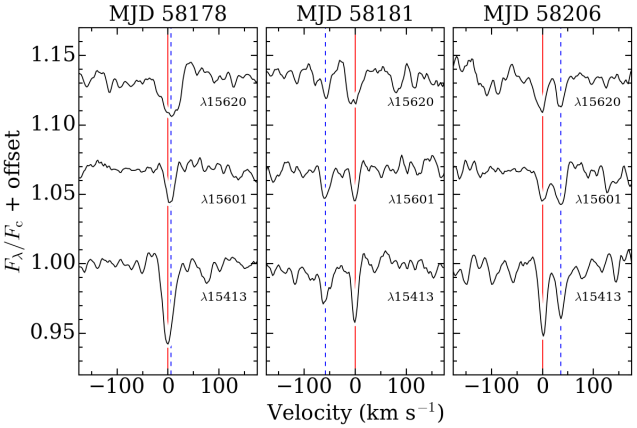

Figure 11. Multiple sets of Mn II lines in the *H*-band spectra of the SB2 2MASS J09432220−5348264 (HD 298641). The Mn II 15413, 15601, and 15620 Å line profiles are shown in the rest frame of the star with stronger Mn II, with a vertical dashed line indicating the position of the secondary star lines.

were detected in the optical but not in the *H*-band. Two of these companions are late-B, rapid rotators, such that we would not expect to see corresponding metal lines in the *H*-band (see the upper two spectra in Figure 2.) Another two of the optical SB2s have cool, faint companions whose *H*-band lines are apparently too weak for detection in APOGEE spectra. Hence, although no convincing evidence is found for lines from companion star(s) in the APOGEE spectra of the SB1s represented in Figure 8, optical spectroscopy will undoubtedly reveal additional SB2s among them, with companions that are too faint, hot, or rapidly rotating to be detected in the *H*-band.

In the following, we discuss the SB2 and SB3 systems individually.

6.3 Binaries with HgMn or Ap/Bp Companions

2MASS J00570626+6134007 = HD 5429 is the clearest available example of an HgMn+Ap/Bp binary, making it the second such system known in addition to HD 161701 (González, et al. 2014). The Ce III lines from the secondary star are quite obvious in the five APOGEE spectra as are numerous lines in our five optical spectra of the system, allowing us to derive the orbital solution shown in Figure 9. With $P = 159$ days and $e = 0.55$, this is one of the widest and most eccentric binaries of the APOGEE HgMn sample. The weakness of the He I lines from the companion in the optical spectra indicates that it is either an late-B or early-A type star, and this is also suggested by the mass ratio ($M_2/M_1 = 0.689$) obtained from the orbital solution. The orbit also suggests a minimum mass of $5.6\,M_\odot$ for the primary, which places it among the most massive HgMn stars.

Figure 10 shows selected regions of the optical spectra, with the left columns demonstrating that both stars produce the low-energy Mn II lines that are numerous in the optical, and with the right column demonstrating that only the Ap/Bp star contributes to doubly-ionized rare earth lines like Pr III and Nd III. The Hg II 3984 Å line of the HgMn primary is among the weakest of our optical sample (see Figure 5), but it is certainly present and without a counterpart from the Ap/Bp star. Instead, the Fe II and Cr II lines of the Ap/Bp star are overly strong, further suggesting that it is a magnetic chemically peculiar star.

2MASS J02060290+5009136 is an SB2 with an Ap/Bp companion that is detected in Ce III 15961 Å in three of the four available APOGEE spectra. The stronger Ce III 16133 Å line is unfortunately blended with residuals from the strong airglow line at 16128 Å, such that we could only measure RVs and estimate $v \sin i$ based on Ce III 15961 Å. The spectra also only cover a short timescale of 21 days, but nonetheless, the Ce III RVs are clearly anti-correlated with those of the Mn II lines, with Ce III going from -41 km s^{-1} to -21 km s^{-1} and with Mn II going from -34 km s^{-1} to -42 km s^{-1}. More spectra will be needed to determine the orbital parameters

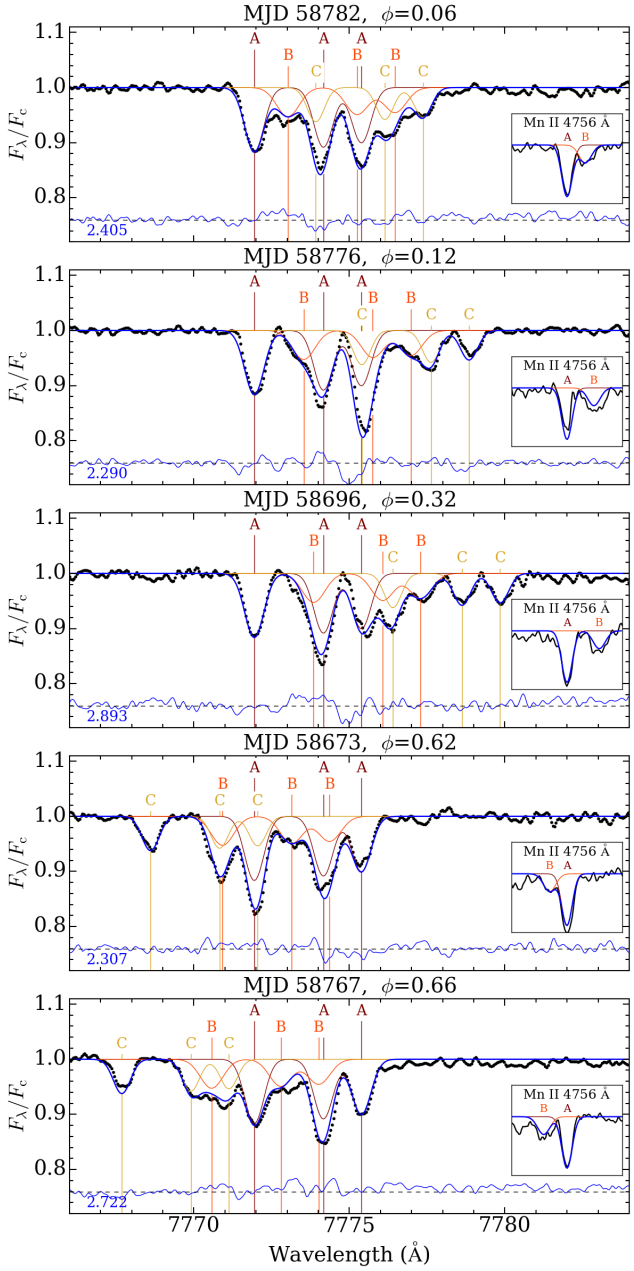

Figure 12. Optical spectra of the HgMn+Bp Mn+Am SB3 2MASS J19223868+1433117 (HD 231263), with the large panels showing the O I triplet (7772, 7774, 7775 Å) blend to which all three stars contribute and with the smaller panels showing an example of the Mn II lines that are produced by the HgMn (A) and Bp Mn (B) stars but not by the Am (C) star. Meanings are otherwise the same as in Figure 10.

of the system and to confirm that is indeed another example of the rare HgMn+Ap/Bp binaries.

2MASS J09432220−5348264 = HD 298641 is the only available example of an HgMn+HgMn binary in which multiple sets of Mn II lines were detected in the APOGEE spectra. Figure 11 shows the Mn II 15413, 15600, and 15620 Å lines from the three spectra, with vertical lines denoting the lines from each star. The components were fully blended on MJD 58178 but well separated on MJDs 58181 and MJD 58206. Although the spectra in Figure 11 are shown in the rest frame of the star that produces stronger Mn II 15413 Å, it is in fact the slightly more RV-variable star (RV_{scat} of 48.6 km s^{-1} versus 46.2 km s^{-1}). Based on the available data, it appears likely that the orbital period is less than 50 days.

2MASS J18064814−2902119 = HD 165347 is a known visual double star with a far fainter companion (5 magnitudes fainter) separated by 6.85″ (Mason, et al. 2001). The 11 APOGEE spectra of the system instead indicate that it is at least an SB3. One of the companions is an Ap/Bp star whose Ce III lines and *UL* (Ce III 15961 Å being the strongest line) are detected in 9/11 spectra, and the other is an A/Am star whose *NSL* (Si I 15964 Å being the strongest line) are detected in 7/11 spectra. The dominant component of the spectra is of course the HgMn star, but over the 6.2 year observational baseline, the Mn II RVs vary by just 10 km s^{-1} with an average of −35 km s^{-1}. The Ap/Bp and A/Am stars are highly RV-variable however, with RV_{scat} of 130 and 133 km s^{-1}, respectively. Figure 9 shows an SB2 orbital solution that suggests they are on a slightly eccentric orbit with P=5.47 days and that the A/Am star is slightly more massive than the Ap/Bp star. The fact that the systemic velocity of the tight SB2 differs from the average RV of the HgMn star by almost 18 km s^{-1} may imply that the HgMn star is on a very long period orbit around either the inner SB2 or a fourth object.

2MASS J19223868+1433117 = HD 231263 is one of the more remarkable discoveries presented here. It is a known visual double star with a companion of comparable brightness (∼ 0.2 magnitude difference) that is separated by just 0.5″ (Mason, et al. 2001). This may be the Am SB2 companion that is detected in C I 16895 Å and the Mg I lines (15753, 15770 Å) in the six APOGEE spectra, but our five optical spectra of the system show that it is actually a multiple system composed of at least three stars. The third star apparently does not produce any strong lines in the *H*-band.

All three stars in the HD 231263 system produce Mg II, Si II, Ti II, Fe II, O I, and Balmer series lines in the optical, and detection of multiple sets of He I lines indicates that the secondary (undetected in the *H*-band) is a late-B type star. Simultaneous detection of Mn II lines (though not Hg II) at the right RVs further indicates that this late-B companion is in fact also an Mn-peculiar star, such that this is an HgMn+Bp Mn+Am system. However, it was the cooler tertiary that was detected in the APOGEE spectra and that is on a circular orbit around the HgMn star. Figure 9 shows the associated SB2 orbital solution, which has a relatively short period of just ∼6.2 days.

Figure 12 shows an attempt to de-blend the O I triplet lines using three sets of Gaussians with fixed equivalent width ratios based on the expected relative strengths of the lines. For the HgMn star, W(7772 Å) was fixed to the value measured from the apparently unblended line on MJD 58696, while for the Am star ('C'), W(7772 Å) was fixed to the average value measured from the apparently unblended lines on MJDs 58673 and 58767. For the Bp Mn star ('B'), the O I wavelengths and widths were fixed based on measurements of Fe II, Si II, and Mg II lines blueward of Hα, and the equivalent widths were simply adjusted until a satisfactory

fit of the full blend was achieved. This resulted in $W(7772\,\text{Å})$ of 90, 48, and 43 mÅ for the A, B and C components, respectively.

The RVs of the Bp Mn star vary by just $4.7\,\text{km s}^{-1}$ over the 109 days covered by the optical spectra, but the average RV of $-7.3\,\text{km s}^{-1}$ is quite close to the $-17.1\,\text{km s}^{-1}$ systemic velocity of the HgMn+Am SB2. It may be the case that the Bp Mn star is on a long period orbit around a fourth star, but it is certainly associated with the SB2.

6.4 Binaries with Am Companions

2MASS J02261624+5704069 = HD 14900 is a known visual double star, with a far fainter companion (4.1 magnitudes fainter) separated by 13″ (Mason, et al. 2001). Although we initially classified this system as an SB1, having found a short orbital period of 4.5 days based on the 10 APOGEE spectra, the companion was clearly detected in three subsequent optical spectra. The strongest line for the companion is Mg II 4481 Å ($W_\lambda = 24$ mÅ), but the Ba II resonance line at 4554 Å is of comparable strength ($W_\lambda = 14$ mÅ), suggesting that the companion is probably an Am star. Both stars are extremely slow rotators with $v \sin i \sim 3$–$4\,\text{km s}^{-1}$. The orbital solution shown in Figure 9 indicates a mass ratio of $q = 0.542$, which is among the smallest of the SB2 systems discussed in this paper. This might explain the *H*-band non-detection of the companion.

2MASS J04502564+6328354 is an SB2 with an Am companion that is clearly detected in the Mg I lines and in C I 16895 Å in the nine available APOGEE spectra and in numerous lines in two optical spectra. An orbital solution of the system is shown in Figure 9, indicating a short period of just 4.3 days and a mass ratio of 0.687. The lack of He I lines at the companion velocities in the two optical spectra confirms the associated A spectral type, and this is further supported by the companion's low-energy Mg I and Fe I lines that lack counterparts from the HgMn star. The SB2 components were well-separated on one of the optical epochs (see Figure 4), allowing for unambiguous identification of number Cr II, Sr II, and Ba II lines from the companion that are quite strong compared to Mg II 4481 Å. For example, the flux ratio of Sr II 4078 Å/Mg II 4481 Å is about 0.4, such that the companion is almost certainly an Am star.

2MASS J05380741+2418520 = HD 37242 is an SB2 in which *NSL* from the Am companion were detected in just one of three APOGEE spectra, with the *NSL* being offset from the Mn II lines by $\sim 166\,\text{km s}^{-1}$ on that epoch. The system was subsequently confirmed as an SB2 by an optical spectrum in which the companion contributions are quite obvious. As with the other SB2s discussed in this section, we classify the companion as an Am star on the basis of overly strong Sr II and Ba II lines. In this case, the equivalent width of the companion's Ba II 4554 Å line is nearly half that of Mg II 4481 Å. Unlike most of the SB2 systems discussed here, the companion ($v \sin i = 15\,\text{km s}^{-1}$) is a far slower rotator than the HgMn star ($v \sin i = 58\,\text{km s}^{-1}$). More spectra will be needed for a full orbital analysis, but based on the large velocity separations of the SB2 components during the two epochs where both were detected, the orbital period is likely to be very short.

2MASS J07144161−1017068 is SB2 with an Am companion whose *NSL* were detected in only two of the five APOGEE spectra. The system is relatively faint ($H = 10.366$) compared to most of the sample, such that the companion's weak lines are only discernible after considerable smoothing of the spectra. Our optical follow-up spectrum confirmed that the system is indeed an SB2, and also that the companion is probably an Am star based on clear detection of the Ba II lines. Both of the stars are extremely slow rotators, with nearly identical $v \sin i$ of $\sim 6\,\text{km s}^{-1}$. Despite only 6 total spectra, the orbital period was constrained to < 10 days by the APOGEE spectra (separated by 17 days) in which the companion was detected. An orbital solution with $e = 0$ and $P = 9.25$ days is shown in Figure 9.

2MASS J17314436−2616112 = HD 158704 is a previously known HgMn star identified as an SB2 by Dolk, Wahlgren & Hubrig (2003). It is a visual double star with a 0.35″ separation Mason, et al. (1999) and a clear SB2 in both the optical and *H*-band. A third companion was identified in the high-contrast images presented by Schöller, et al. (2010), and based on the relatively constant RVs (RV_{scat} of $5.7\,\text{km s}^{-1}$ across 2 APOGEE spectra and 3 optical spectra) of of the HgMn star, we suspect that this is indeed a multiple system. The slowly-rotating Am companion is certainly RV-variable however, with $\text{RV}_{\text{scat}} = 37.8\,\text{km s}^{-1}$.

2MASS J20360994+3929487 is one of the more obvious SB2s of the sample, with numerous narrow *NSL* detected in the 6 APOGEE spectra. The companion is a slowly-rotating star with $v \sin i \sim 11\,\text{km s}^{-1}$, and considering the relative weakness of its lines in the optical, it may be the coolest SB2 secondary of the sample. For example, attempts to deblend the contributions to Mg II 4481 Å from the two stars indicates that the companion line is perhaps only 10% as strong the HgMn star line. Nonetheless, Ba II lines from the companion are clearly present in the spectra at strengths comparable to Mg II 4481 Å, such that we classify it as an Am star. Figure 9 shows an orbital solution with a 31.4 day period and a relatively high eccentricity of $e = 0.58$. The mass ratio of $M_2/M_1 = 0.536$ is the lowest reported in this paper.

2MASS J23575323+5723194 = HD 224435 is another known visual multiple system, with at least two companions separated by 1.2″ and 8.7″, respectively (Mason, et al. 2001). The more distant companion is about 3.8 magnitudes fainter than the HgMn star, but the close companion is only 0.2 magnitudes fainter and hence is presumably the SB2 companion detected in the 18 APOGEE spectra and 4 optical spectra. The companion is a slow rotator with $v \sin i \sim 11\,\text{km s}^{-1}$ and with the Mg I and C I lines being the strongest *H*-band features. As with the other stars discussed in this section, we classify the companion as Am based on clear detection of Sr II and Ba II lines that are comparable in strength to Mg II 4481 Å. Despite the Am star being highly RV-variable, the RVs of the HgMn star vary by only $\sim 13\,\text{km s}^{-1}$ over the 8.2 year observational baseline, with variation pattern seeming unrelated to the motion of the Am star. Figure 9 shows an SB1 orbital solution for the Am star, with the HgMn star RVs phased to the 21 day period. The average RV of the HgMn star is quite close to the systemic velocity indicated by the SB1 orbit of the Am star

(-10.7 km s^{-1} versus -7.2 km s^{-1}), such that the two stars are certainly associated.

6.5 Other SB2s and SB3s

2MASS J02203397+6023494 is a likely multiple system. The spectrum of an A/Am star was detected in all 11 APOGEE spectra, with the RVs varying by 11 km s^{-1}. The HgMn star RVs are even more highly RV-variable, with the maximum difference between epochs being 18 km s^{-1}. Despite this, we could not find reasonable orbital solutions for either star and certainly not for an SB2 combination since the relative RV variability seems random.

2MASS J04315476+2138086 = HD 28662 is a definite SB2 with an A or Am companion that is the fastest rotator ($v \sin i \sim 62$ km s^{-1}) of all the *H*-band-detected secondary stars described in this paper. In the single APOGEE spectrum of the system, the companion is most clearly detected in the Mg I lines between 15745–15770 Å and in C I 16895 Å, with those lines being offset from Mn II by roughly 149 km s^{-1}.

2MASS J04510073+3226501 = HD 30661 is another SB2 in which the companion was detected in optical spectra but not in the APOGEE spectra. An SB2 orbital solution shown in Figure 9, and the associated mass ratio of $q = 0.895$ is the largest reported here. The optical data show that the stars are near spectroscopic twins in terms of almost identical $v \sin i$ and almost identical depths and strengths of the Balmer series, Si II, Fe II, Ti II, Mg II, and O I lines (among other species). The two most striking differences between the two stars are the lack of Mn II, Hg II, and other heavy metal lines from the companion star, as well as the relative strength of the He I lines for the two stars. Namely, the He I 5876 Å equivalent width of the HgMn star is about half that of the companion. This would normally suggest that the companion is in fact the hotter, more massive star, but in this case it is almost certainly due to a severe depletion of He for the HgMn star.

2MASS J06402199−0322092 = HD 47798 is a visual double star confirmed by Mason, et al. (1999). We measured RVs from possible weak *NSL* features in the three APOGEE spectra covering 57 days, indicating that there may be an A/Am companion. However, the resulting RVs are a good match to those of the HgMn star, with the averages being 22 km s^{-1} and 23 km s^{-1}, respectively. The RV$_{\rm scat}$ is also small for both, at 5.5 km s^{-1} for the HgMn star and 2.5 km s^{-1} for the A/Am star. This may be a long-period SB2 or a multiple system.

2MASS J06561603−2839053 = HD 51459 is another SB2 with an A/Am companion. In the single APOGEE observation, the RVs of the HgMn and A/Am components were 65 km s^{-1} and −79 km s^{-1}, respectively. Relatively strong Ce III lines (e.g, Ce III 15961 Å/Mn II 15413 Å ∼ 0.53) are present in the spectra, but their RVs and FWHM are all but identical to those of the Mn II lines.

2MASS J06572439−0928136 = HD 51539 is another SB2 with an A/Am companion that is clearly detected in the 3/4 available APOGEE spectra with sufficient S/N. The RVs of the HgMn and A/Am star vary by just 4.4 km s^{-1} and 2.5 km s^{-1}, respectively, in the three spectra taken over 50 days, but the variability is anti-correlated.

2MASS J14482274−5959316 = HD 130039 was included in the sample due to fairly confident detection of Mn II 15413 and 15620 Å in the first of three APOGEE spectra (MJD 58657). That spectrum also exhibits numerous *NSL* (indicating an A/Am spectral type) at an RV of 98 km s^{-1} as compared to the Mn II RV of 0 km s^{-1}. The Mn II lines are not confidently detected in the subsequent two spectra (MJDs 56677 and 56689), but the A/Am star RVs drop to −23 km s^{-1} and then −133 km s^{-1} in those spectra. This is certainly an SB system, but it is unclear whether it actually involves an HgMn star. It is a known visual double star with a small separation of 0.56″, but the visual companion is 4.24 magnitudes fainter than the primary star (Horch, et al. 2015).

2MASS J16133258−6019519 is a likely SB2 with an A/Am companion. The Mg I lines at 15753 and 15770 Å seem to definitely be present in the spectra, but disagreement of the RVs of the lines renders the result ambiguous. The HgMn star is only marginally RV-variable.

2MASS J18391486+2029512 = HD 172397 has a late-B SB2 companion that was detected in our five optical follow-up spectra but not in the seven APOGEE spectra. The *H*-band non-detection is almost certainly due in part to the relatively rapid rotation of the companion; based on fitting multiple Gaussians to the partially blended Si II 3863 Å, Mg II 4481 Å, and Fe II 5169 Å lines in one of the optical spectra, we estimate that the companion has $v \sin i \sim 70$ km s^{-1}. Any *H*-band metallic features from the star would be quite weak to begin with, and probably undetectable for such a rapid rotator. The ratio of the equivalents of He I 4471 Å over Mg II 4481 Å for the companion is not much less than unity, indicating that it is definitely hotter than A0. The lack of detectable metal absorption features from the companion in the *H*-band is therefore unsurprising (see Figure 2). Figure 9 shows a possible SB2 orbit with a 35 day period and $e = 0.36$.

2MASS J19294384−1801510 = HD 183327 has an A/Am companion whose *NSL* are quite obvious and offset from the Mn II lines by ∼ 13 km s^{-1} in the single APOGEE spectrum.

2MASS J19454054+3959248 = HD 225692 has a broad-lined companion that was detected in our three optical spectra but not in the 13 APOGEE spectra. The broad components are most obvious in the He I lines and Mg II 4481 Å, with weaker contributions in the Si II and O I lines, indicating that it is a late-B type star. Based on attempts to fit Gaussians to the blended He I 4471 Å and Mg II 4481 Å region, we estimate that the companion has $v \sin i \sim 200$ km s^{-1}. Thus, it is not terribly surprising that we see no evidence of this star in the APOGEE spectra, since it might not produce significant metal absorption lines even if was not such a rapid rotator. The orbital solution shown in Figure 9 indicates $P = 338$ days, which matches the period found if we treat the system as an SB1, and which is by far the longest orbital period reported in this paper. The mass ratio of the SB2 orbital solution ($M_2/M_1 = 0.538$) is

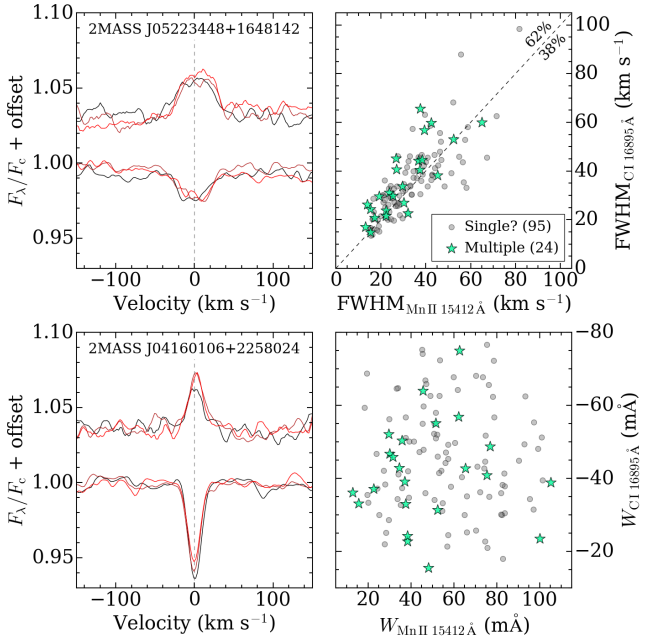

Figure 13. (*Left panels:*) Demonstration of the matching radial velocities and line widths of Mn II 15413 Å absorption and C I 16895 Å emission. Each panel shows spectra from three epochs, corrected to rest frame based on the Mn II radial velocities and with the C I region artificially shifted upward. 2MASS designations are given above each panel. (*Upper right:*) The FWHMs of Mn II 15413 Å versus those of C I 16895 Å, with the dotted line indicating $y = x$. (*Lower right:*) The equivalent widths of the same lines. Star symbols indicate binary and multiple systems.

among the lowest reported in this paper, which is surprising considering that the companion is a B-type star.

7 CARBON EMISSION

As mentioned in Section 3 and Figure 2, HgMn stars often exhibit conspicuous narrow emission in the C I 16895 Å line. More specifically, this is true for roughly 45% of the sample (120 stars). Only in cases of exceptionally strong C I 16895 Å emission are the weaker C I lines at 16009 and 16026 Å (labeled in Figure 2) observed in emission. To confirm that the emission is in fact associated with the HgMn stars rather than being some kind of spurious artifact, we fit Gaussians to the C I emission features in order to obtain estimates of the RV, FWHM, and equivalent width of the feature.

Based on this, our first conclusion regarding the nature of the line emission is demonstrated in the two lefthand panels of Figure 13. These panels show the Mn II 15413 Å (lower lines) and C I 16895 Å (upper lines) line profiles from three epochs for two stars that exemplify the behavior of these lines. The spectra have been shifted to rest frame based on the RVs of the Mn II lines, making it clear that the C I emission occurs at roughly the same RVs is therefore definitely associated with the HgMn stars. However, small blueshifts (1–5 km s^{-1}) of the C I emission peaks are visible in most of the displayed spectra, indicating that the emission forms just above the surfaces of the stars.

Our second conclusion is the one made obvious by inspection of the line profile widths in lefthand panels of Figure 13, and then quantified in the upper right panel, which plots the FWHM of the C I 16895 Å emission versus the FWHM of Mn II 15413 Å. There is considerable scatter about the $y = x$ line, with 62% of the stars having C I wider than Mn II, but the suggestion is nonetheless that the C I emission exhibits the same level of broadening as the Mn II lines and is therefore definitely associated with the surfaces of the stars. The same conclusions were reached by Wahlgren & Hubrig (2000) with respect to narrow emission lines in the optical spectra of chemically normal and chemically peculiar late-B stars.

As far as correlations with other spectral features, there are none to be found in the APOGEE spectra. The lower right panel of Figure 13 plots the equivalents widths of Mn II 15413 Å versus those of C I 16895 Å, showing that the strength of the C I emission has no dependence on the strength of the Mn II absorption lines. There also does not seem to be a correlation between C I emission and binarity, since the fraction of stars with C I emission that are definitely binaries or multiples (20%) is considerably lower than the 31% binary fraction for the full sample.

Emission in the C I 16895 Å line is certainly not a

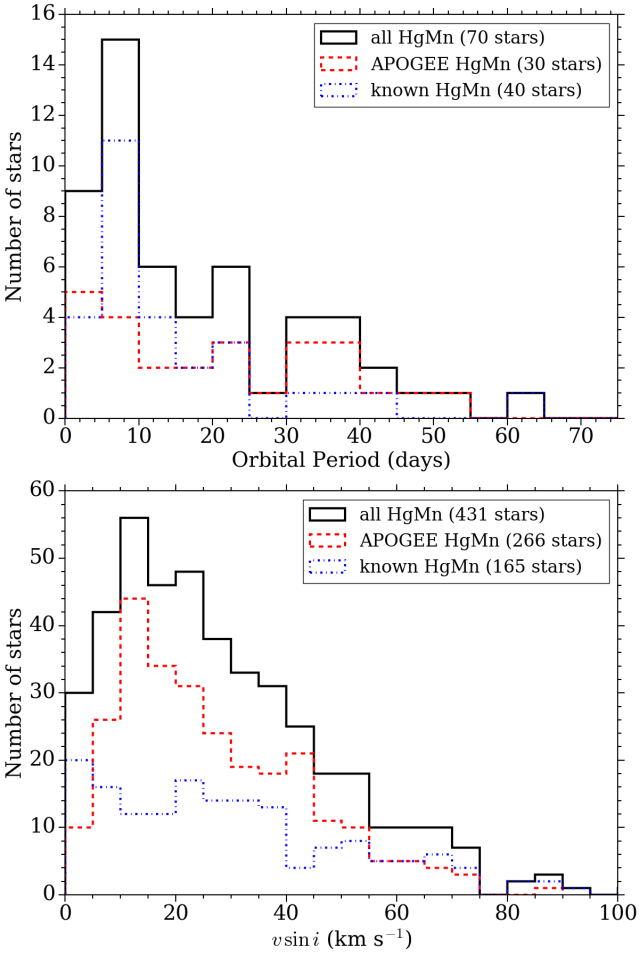

Figure 14. Histogram of orbital periods for HgMn binaries. The solid line indicates the APOGEE sample, and the dashed line indicates the known sample.

rare phenomenon and is not limited to chemically peculiar stars; recall that the B8 V star HD 2559 exhibits C I emission in the spectrum shown in Figure 2. C I emission is also present in $\sim 20\%$ of the classical Be star spectra obtained by APOGEE (Chojnowski, et al. 2015), and the emission is particularly strong in the case of exotic binaries such as Be+sdO (HD 55606; Chojnowski, et al. 2018) and Be+black hole (HD 215227; unpublished data). The C I 16895 Å line is also observed in emission in the spectra of blue supergiants (e.g., HD 15266), pre-main-sequence, supergiant, and unclassified B[e] stars (e.g., MWC 361, MWC 137, and MWC 922), luminous blue variables (e.g., S Doradus), post-AGB stars (e.g., IRAS 05040+4820), and extreme Helium stars (e.g., V2244 Oph).

8 DISCUSSION

Thanks to the strategy of selecting as telluric standards thousands of blue stars across the sky down to $H = 11$, the APOGEE survey has more than doubled the known sample of HgMn stars, expanding it from ~ 194 stars to a grand total of just over 450 stars. Although still quite rare, we estimate that somewhere between 5–10% of the late-B stars observed by APOGEE are in fact HgMn stars. This significant increase of the sample of HgMn stars promises to open new perspectives for our knowledge and understanding of mid to late-main sequence B-type stars, and some inferences can already be made based on the basic analysis presented in this paper.

Combining the 30 orbital solutions for new HgMn stars with the 40 orbital solutions for known HgMn stars in the 9th Catalogue of Spectroscopic Binary Orbits (Pourbaix et al. 2009), we have orbital period estimates for a total of 70 HgMn binaries. Of these systems, 57/70 (77%) have periods less than 75 days, 54/70 (74%) have periods less than 50 days, and 40/70 (57%) have periods less than 25 days. This result is emphasized in the upper panel of Figure 14, which shows that the distribution of orbital periods (excluding the 16 systems with $P > 75$ days) is strongly peaked in the 5–10 day range. The previously suggested preference for short orbital periods (Hubrig & Mathys 1995) is therefore confirmed.

The lower panel of Figure 14 shows the distribution of $v \sin i$ for HgMn stars, confirming that HgMn stars are slow rotators as a rule. The overall average is $<v \sin i>= 28\,\mathrm{km\,s^{-1}}$ and the distribution is strongly peaked toward $v \sin i \sim 20\,\mathrm{km\,s^{-1}}$. For comparison, the average $v \sin i$ of non-supergiant, B7–A0, apparently chemically normal stars included in the catalog of Abt, Levato & Grosso (2002) is $> 120\,\mathrm{km\,s^{-1}}$. The phenomenon of B-type stars exhibiting HgMn abundance anomalies is therefore intimately linked not only with their multiplicity but with their slow rotation. These are key ingredients in the formation of HgMn stars.

ACKNOWLEDGEMENTS

Funding for the Sloan Digital Sky Survey IV has been provided by the Alfred P. Sloan Foundation, the U.S. Department of Energy Office of Science, and the Participating Institutions. SDSS acknowledges support and resources from the Center for High-Performance Computing at the University of Utah. The SDSS web site is www.sdss.org.

SDSS is managed by the Astrophysical Research Consortium for the Participating Institutions of the SDSS Collaboration including the Brazilian Participation Group, the Carnegie Institution for Science, Carnegie Mellon University, the Chilean Participation Group, the French Participation Group, Harvard-Smithsonian Center for Astrophysics, Instituto de Astrofísica de Canarias, The Johns Hopkins University, Kavli Institute for the Physics and Mathematics of the Universe (IPMU) / University of Tokyo, Lawrence Berkeley National Laboratory, Leibniz Institut fur Astrophysik Potsdam (AIP), Max-Planck-Institut fur Astronomie (MPIA Heidelberg), Max-Planck-Institut fÃijr Astrophysik (MPA Garching), Max-Planck-Institut fÃijr Extraterrestrische Physik (MPE), National Astronomical Observatories of China, New Mexico State University, New York University, University of Notre Dame, ObservatÃşrio Nacional / MCTI, The Ohio State University, Pennsylvania State University, Shanghai Astronomical Observatory, United Kingdom Participation Group, Universidad Nacional Autónoma de México, University of Arizona, University of Colorado Boulder, University of Oxford, University of Portsmouth, University of Utah, University of Virginia, University of Washington, University of Wisconsin, Vanderbilt University, and Yale University.

S.H. is supported by an NSF Astronomy and Astrophysics Postdoctoral Fellowship under award AST-1801940. DAGH acknowledges support from the State Research Agency (AEI) of the Spanish Ministry of Science, Innovation and Universities (MCIU) and the European Regional Development Fund (FEDER) under grant AYA2017-88254-P.

REFERENCES

Abt H. A., Levato H., Grosso M., 2002, ApJ, 573, 359
Aguado D. S., et al., 2019, ApJS, 240, 23
Alecian G., Gebran M., Auvergne M., Richard O., Samadi R., Weiss W. W., Baglin A., 2009, A&A, 506, 69
Andrews J. J., Chanamé J., Agüeros M. A., 2017, MNRAS, 472, 675
Blanton M. R., et al., 2017, AJ, 154, 28
Bowen I. S., Vaughan A. H., 1973, ApOpt, 12, 1430
Briquet M., Korhonen H., González J. F., Hubrig S., Hackman T., 2010, A&A, 511, A71
Ćalıskan Ş., Ünal Ö., 2017, AIPC, 140001, AIPC.1815
Castelli F., Hubrig S., 2004, A&A, 425, 263
Chojnowski S. D., et al., 2015, AJ, 149, 7
Chojnowski S. D., et al., 2018, ApJ, 865, 76
Chojnowski S. D., et al., 2019, ApJ, 873, L5
Cowley C. R., Aikman G. C. L., 1975, PASP, 87, 513
Dolk L., Wahlgren G. M., Hubrig S., 2003, A&A, 402, 299
Eisenstein D. J., et al., 2011, AJ, 142, 72
Ghazaryan S., Alecian G., 2016, MNRAS, 460, 1912
Ghazaryan S., Alecian G., Hakobyan A. A., 2018, MNRAS, 480, 2953
González J. F., Levato H., 2009, RMxAC, 300, RMxAC..35
González J. F., et al., 2014, A&A, 561, A63
Gunn J. E., et al., 2006, AJ, 131, 2332
Horch E. P., van Belle G. T., Davidson J. W., Ciastko L. A., Everett M. E., Bjorkman K. S., 2015, AJ, 150, 151

Hubrig S., Mathys G., Comments Astrophys., 18, 167
Hubrig S., Castelli F., Wahlgren G. M. 1999, A&A, 346, 139
Hubrig S., et al., 2010, MNRAS, 408, L61
Hubrig S., et al., 2012, A&A, 547, A90
Hubrig S., et al., 2014, MNRAS, 440, L6
Hümmerich S., Niemczura E., Walczak P., Paunzen E., Bernhard K., Murphy S. J., Drobek D., 2018, MNRAS, 474, 2467
Kervella P., Arenou F., Mignard F., Thévenin F., 2019, A&A, 623, A72
Korhonen H., et al., 2013, A&A, 553, A27
Majewski S. R., et al., 2017, AJ, 154, 94
Malanushenko V. P., 1996, Ap, 39, 208
Makaganiuk V., et al., 2011, A&A, 529, A160
Makaganiuk V., et al., 2012, A&A, 539, A142
Mason B. D., et al., 1999, AJ, 117, 1890
Mason B. D., Wycoff G. L., Hartkopf W. I., Douglass G. G., Worley C. E., 2001, AJ, 122, 3466
Mathys G., Hubrig S., 1995, A&A, 293, 810
Monier R., Gebran M., Royer F., 2015, A&A, 577, A96
Monier R., Gebran M., Royer F., 2016, sf2a.conf, 213, sf2a.conf
Monier R., Gebran M., Royer F., Kılıcoğlu T., 2017, sf2a.conf, Di, sf2a.conf
Nidever D. L., et al., 2015, AJ, 150, 173
Pourbaix D., et al., 2004, A&A, 424, 727
Pourbaix D., Tokovinin A. A., Batten A. H., et al. 2009, A&A, 424,72
Renson P., Manfroid J., 2009, A&A, 498, 961
Ryabchikova T., 1998, CoSka, 27, 319
Ryabchikova T. A., Malanushenko V. P., Adelman S. J., 1999, A&A, 351, 963
Iglesias-Marzoa R., López-Morales M., Jesús Arévalo Morales M., 2015, PASP, 127, 567
Schneider H., 1981, BICDS, 20, 113
Schöller M., Correia S., Hubrig S., Ageorges N., 2010, A&A, 522, A85
Simón-Díaz S., Herrero A., 2014, A&A, 562, A135
Skrutskie M. F., et al., 2006, AJ, 131, 1163
Smith K. C., Dworetsky M. M., 1993, A&A, 274, 335
Tsymbal V. V., Kotchukhov O. P., Khokhlova V. L., Lambert D. L., 1998, AstL, 24, 90
Wahlgren G. M., Hubrig S., 2000, A&A, 362, L13
Wang S.-. i ., et al., 2003, SPIE, 1145, SPIE.4841
White R. E., Vaughan A. H., Preston G. W., Swings J. P., 1976, ApJ, 204, 131
Wilson J. C., et al., 2019, PASP, 131, 055001
Zasowski G., et al., 2013, AJ, 146, 81
Zasowski G., et al., 2017, AJ, 154, 198

Table 4. APOGEE HgMn Stars

2MASS Designation	Other Name	2MASS H (mag)	<S/N>	$N_{RV}/N_{obs.}$	$v \sin i$ (km s^{-1})	$<W_\lambda>$ Mn II 15413 (mÅ)	$<W_\lambda>$ Ce III 15961 (mÅ)	$<W_\lambda>$ C I 16895 (mÅ)	<RV> (km s^{-1})	$RV_{scat.}$ (km s^{-1})	Binary Type	Literature Spectral Type
00091817+7022314	...	8.953	216	12/12	17 ± 8	35	...	-33	-19.1 ± 2.1	4.7	...	...
00245787+6212255	...	10.479	112	11/12	4 ± 4	23	...	-37	-29.5 ± 2.8	7.0	SB1	...
00364423+5810121	...	10.345	109	7/12	62 ± 2*	61	...	...	-31.5 ± 7.5	21.9	...	...
00390709+5558188	...	10.472	109	6/6	36 ± 7	54	...	...	-21.5 ± 5.4	2.6	...	...
00570626+6134007	HD 5429	8.403	268	10/10	20 ± 2*	30	...	-47	-3.2 ± 2.2	62.5	SB2*	B8 III[1]
01011057+6355294	Hilt 91	9.860	140	3/3	10 ± 4	82	...	-30	-28.2 ± 1.1	1.3	...	B9 III:[1]
01165086+5902504	...	9.709	129	4/4	59 ± 5	62	...	...	-15.5 ± 7.4	7.8	...	B8[1]
01191843+5902478	HD 7844	8.317	261	5/5	39 ± 2*	79	...	-72	-29.1 ± 2.0	4.3	...	B8[1]
01494647+5653549	...	10.600	88	3/3	15 ± 5	33	...	...	-31.8 ± 6.3	5.7	...	...
01533081+5736078	...	10.507	103	3/3	38 ± 8	56	13	...	-52.9 ± 6.4	6.7	...	...
01573735+3729276	Renson 3040	9.678	...	3/3	...	...	...	...	12.0 ± 4.9	9.5	...	A0 HgMn[2]
01590590+6132312	HD 11918	7.720	388	9/9	13 ± 2*	36	...	-50	-3.8 ± 1.8	26.2	SB1*	B9 IV[1]
02030138+6103545	HD 12340	8.740	262	7/7	60 ± 2*	45	...	...	-14.2 ± 7.1	25.0	...	B9 III[1]
02060290+5009136	...	10.411	106	4/4	33 ± 4	51	23	-50	-38.0 ± 6.4	8.3	SB2	...
02063211+6056171	...	9.023	218	6/6	11 ± 4	95	...	-34	-8.4 ± 1.2	1.6	...	...
02154357+5607505	HD 13736	9.002	222	3/3	16 ± 7	53	23	-72	-35.3 ± 3.8	3.2	...	B9 V[1]
02183895+5622346	HD 14093	8.375	217	12/12	19 ± 1*	71	41	-62	-31.6 ± 1.6	5.6	...	B9 III[1]
02203397+6023494	...	9.872	122	11/11	27 ±10	62	...	...	-16.1 ± 3.4	21.6	SB2	...
02231800+5903056	...	10.201	88	10/10	21 ± 6	51	...	-52	-16.1 ± 1.9	8.9	...	B8 IV[1]
02232391+5651153	HD 14581	8.191	286	12/12	3 ± 2*	52	...	-55	-10.0 ± 1.0	29.6	SB1*	B8 Si[2]
02261624+5704069	HD 14900	8.318	267	13/13	3 ± 2*	30	...	-52	-22.1 ± 1.9	115.8	SB2*	B9 V[1]
02270546+6239287	BD+62 396	9.922	112	12/12	29 ± 5	71	...	-43	-35.4 ± 3.2	7.0	...	B[1]
02371246+6025140	...	9.726	145	5/5	39 ± 6	45	...	-75	-49.7 ± 5.7	11.2	...	B9 V[1]
02431092+6135575	NGC 1027 5	10.485	118	1/1	43 ± 9	62	...	...	-16.4 ± 6.9	...	...	B9 V[1]
02463385+6039445	...	10.889	102	1/1	29 ±11	56	...	...	-43.5 ± 1.0	...	...	B9 V[1]
02511226+6133221	BD+60 577	9.863	174	3/3	10 ± 5	32	...	-46	-22.2 ± 2.9	21.4	SB1	B/A[1]
02515823+6506469	...	10.089	139	3/3	41 ± 5	59	...	...	-19.7 ± 6.7	12.3	...	...
02520460+6220449	...	10.267	119	3/3	23 ± 5	49	...	...	-35.3 ± 4.1	1.6	...	B8 V[1]
03031960+6509437	HIP 14216	8.456	292	4/4	41 ± 4	46	...	...	-20.3 ± 6.2	78.3	SB1	B5[1]
03032447+4355547	...	10.648	77	6/7	29 ± 4	38	...	-57	-12.7 ± 4.3	13.1	...	...
03070819+5741417	...	9.512	136	7/7	37 ±10	49	...	...	-18.0 ± 5.8	8.1	...	...
03072912+5406408	HD 19195	7.738	439	3/3	51 ± 6	38	...	...	-4.3 ± 6.7	14.7	...	B9[1]
03111800+4713310	HD 19625	9.053	167	7/7	61 ± 9	60	...	...	-18.4 ± 8.4	39.6	...	A[1]
03140847+4007085	HD 19981	7.150	396	10/10	17 ± 1*	51	22	...	10.0 ± 1.4	53.4	SB1*	B9[1]
03291593+6311118	...	9.382	179	3/3	46 ±11	61	...	...	-13.9 ± 4.5	5.5	...	...
03395650+5519593	...	10.456	101	5/6	52 ± 4	81	...	...	-13.8 ± 4.7	16.3	...	...
03470474+6118534	...	10.107	120	3/3	17 ± 6	47	...	-36	-15.9 ± 3.6	1.7	...	...
04153412+4939456	...	9.241	177	6/6	12 ± 5	52	...	-58	-14.2 ± 2.5	4.3	...	...
04160106+2258024	HD 26910	8.386	304	5/5	5 ± 4	56	...	-44	-11.3 ± 1.7	1.3	...	A[1]
04203306+2839085	HD 283567	9.406	164	8/8	53 ± 6	66	...	...	-5.6 ± 5.7	22.4	...	B9[1]
04213140+6047336	HD 27223	8.076	340	6/6	34 ± 9	46	...	-48	-5.9 ± 3.3	5.5	...	B9[1]
04222106+4530170	BD+45 924	9.313	198	3/3	64 ±12	52	...	...	-47.7 ± 6.5	23.4	...	B8[1]
04222649+3654202	HD 27548	7.685	448	1/1	27 ± 5	123	...	...	5.2 ± 1.3	...	...	B9[1]
04272207+2935073	HD 282176	10.243	121	6/6	15 ± 5	93	...	-63	-18.4 ± 2.2	9.3	...	A[1]
04291488+2228426	HD 284479	10.067	99	1/1	6 ± 6	47	...	-67	-58.2 ± 1.1	...	...	A1[1]
04315476+2138086	HD 28662	7.726	237	1/1	63 ± 8	101	...	...	-39.0 ± 9.3	...	SB2	A2[1]
04333888+5237552	HD 232975	8.825	228	3/3	11 ± 4	62	...	-64	-21.7 ± 2.5	3.6	...	B5[1]
04374394+4141338	HD 276610	9.743	153	3/3	42 ± 5	76	...	-66	-27.7 ± 7.6	6.9	...	A0 III[1]
04391676+3240441	none	10.559	74	3/3	33 ± 4	67	...	...	-14.7 ± 6.2	3.5	...	...
04451797+1912411	HD 284844	9.189	128	1/1	29 ±11	39	...	-35	-13.9 ± 4.2	...	...	A0[1]
04482628+2436124	...	9.831	159	1/1	5 ± 4	101	32	-51	0.3 ± 1.0	...	...	...
04495425+3220267	HD 282459	8.842	201	3/7	42 ± 9	28	...	...	-11.3 ±10.0	29.0	...	B9[1]
04501014+4402596	HD 30481	8.837	224	7/7	20 ± 4	57	...	-49	-27.0 ± 3.4	4.1	...	A0 III[1]
04502564+6328354	BD+63 538	9.021	156	11/11	22 ± 2*	47	...	...	-18.1 ± 4.7	136.7	SB2*	A0[1]
04510073+3226501	HD 30661	8.405	235	9/9	13 ± 3*	41	...	...	13.5 ± 1.8	139.3	SB2*	A0[1]
04511614+3349189	HD 282491	8.968	173	4/7	26 ±11	19	...	-69	-18.0 ± 5.8	16.8	...	A2[1]
04572691+3010291	HD 282633	8.749	179	4/4	11 ± 2*	33	...	...	-2.0 ± 5.7	9.7	...	B8[1]
04585415+2258203	HD 284958	10.273	97	6/12	40 ± 4	28	...	-38	-14.0 ± 3.7	17.1	...	A0[1]
05014768+2146215	HD 285025	9.716	117	8/12	26 ± 4	16	...	-33	14.7 ± 5.3	78.6	SB1*	B8[1]
05075830+4559188	BD+45 1045	9.774	105	5/5	29 ± 5	93	...	-49	-7.3 ± 2.6	2.8	...	B8 V[1]
05081080+4533225	...	10.461	65	3/5	59 ± 4	110	...	...	-29.9 ±10.0	8.8	...	...
05140453+3919226	HD 277813	10.755	89	10/11	23 ± 4	34	...	...	-9.1 ± 6.5	9.2	...	B5[1]
05180389+4449047	HD 34236	9.033	195	14/14	20 ± 5	51	...	-55	-7.0 ± 2.8	7.6	...	A0[1]
05193355+2846259	HD 34546	8.647	253	3/3	19 ± 5	36	17	-34	-14.6 ± 4.8	2.0	...	B9[1]
05223448+1648142	HD 35051	7.769	426	3/3	31 ± 5	45	...	-74	-4.5 ± 4.6	4.0	...	B8 V[1]
05232293−0126272	HD 290385	8.480	301	2/2	75 ± 5	64	...	...	35.0 ±10.0	8.5	...	A0[1]
05253107−0032383	HD 35548	6.644	594	6/6	10 ± 4	17	26	-59	-9.9 ± 2.6	3.6	...	B9 III[1]
05285946+2548477	...	9.905	142	14/14	14 ± 4	57	...	-25	-2.1 ± 1.7	3.4	...	...
05301034−0512058	HD 36234	8.825	188	6/6	5 ± 4	66	...	-25	19.5 ± 1.0	3.1	...	B9 III[1]
05320399−0025448	BD−00 984	8.673	243	8/8	40 ± 7	77	...	...	19.1 ± 3.6	19.3	...	B8 III[1]
05323948+0205318	HD 36549	8.725	237	1/1	50 ± 5	88	...	...	44.2 ± 5.5	...	...	B7 He wk[2]

[1] SIMBAD
[2] Renson 2009

Table 4 – *continued*

2MASS Designation	Other Name	2MASS H (mag)	<S/N>	$N_{RV}/N_{obs.}$	$v \sin i$ (km s^{-1})	<W_λ> Mn II 15413 (mÅ)	<W_λ> Ce III 15961 (mÅ)	<W_λ> C I 16895 (mÅ)	<RV> (km s^{-1})	$RV_{scat.}$ (km s^{-1})	Binary Type	Literature Spectral Type
05342016+2556549	...	10.985	78	12/14	13 ± 8	38	...	-33	5.5 ± 3.9	15.5	SB1	...
05344815+3911379	BD+39 1341	9.733	139	3/3	19 ± 5	26	...	...	-9.0 ±10.0	5.9	...	A0[1]
05354435+4529356	HD 36662	8.261	269	9/9	18 ± 5	52	...	-52	-27.9 ± 5.4	15.8	...	B8 MnHg[2]
05355825+0931541	HD 37035	8.712	201	11/12	38 ± 4	46	...	...	22.8 ± 8.3	18.1	...	B9 V[1]
05362280+3219581	HD 36892	8.506	262	8/8	20 ± 1*	62	...	-57	-1.1 ± 2.1	87.9	SB1*	A2[1]
05364286+2402058	...	10.113	115	2/4	29 ±10	48	...	...	-3.1 ± 6.9	4.8	...	...
05380741+2418520	HD 37242	9.064	189	4/4	58 ± 3*	80	...	...	0.6 ± 7.1	119.3	SB2	A[1]
05381875+3742428	BD+37 1263	8.863	213	3/3	11 ±11	13	...	-36	-1.0 ± 4.7	98.3	SB1	A2[1]
05382578+3253567	...	10.139	129	8/9	32 ± 7	31	...	...	-9.6 ± 7.8	13.2	...	...
05384609+4434392	BD+44 1258	9.286	170	9/9	14 ± 4	75	26	-38	-11.3 ± 2.5	3.4	...	B9 V[1]
05400356+3153578	HD 37437	7.951	338	10/10	17 ± 1*	79	...	-57	1.3 ± 1.4	11.9	...	B9[1]
05403287+3311244	HD 246021	9.876	112	9/9	15 ± 5	57	...	...	-11.5 ± 2.5	16.2	SB1*	...
05431969+5315593	...	10.268	97	9/11	21 ± 5	28	...	-25	-23.9 ± 6.3	9.0	...	...
05463674+4516176	BD+45 1169	9.383	164	9/9	51 ± 8	82	...	-36	-22.9 ± 6.5	20.7	...	B8 II[1]
05464904+1212013	...	10.302	126	3/9	32 ±11	20	...	-33	23.6 ± 7.2	15.0	...	...
05510374+3403257	BD+34 1190	8.920	210	3/3	20 ± 5	75	...	-45	5.8 ± 2.7	1.7	...	...
05513245+2815280	HD 248343	9.321	164	12/12	20 ± 5	46	...	-60	-5.9 ± 3.3	9.2	...	...
05530948+2654242	...	10.093	99	10/10	45 ± 5	126	...	-59	-12.0 ± 3.5	33.4	SB1*	...
05542138+5215443	HD 39271	8.526	221	8/8	3 ± 2*	44	26	-23	-26.1 ± 1.2	16.0	SB1*	B9[1]
05572511+2412019	HD 249531	9.752	146	7/7	26 ± 5	65	...	-30	-3.7 ± 4.1	6.7	...	B8[1]
05574495+2550281	HD 249589	10.101	121	10/10	33 ± 5	76	...	-21	-12.0 ± 3.3	8.5	...	B8[1]
06023873+2951054	...	10.848	88	13/14	14 ± 5	30	...	-29	-11.6 ± 2.9	6.9	...	...
06025889+1338101	...	10.725	96	12/12	34 ± 7	57	...	...	5.2 ± 5.4	15.2	...	...
06051550+3045489	...	9.620	155	15/15	17 ± 6	48	...	-16	-16.1 ± 2.2	36.9	SB1*	...
06070692+2303141	HD 41592	8.373	282	13/13	38 ±2*	28	...	...	-6.6 ± 6.5	45.2	SB1	B9[1]
06081031+2454284	HD 41766	9.311	202	4/4	43 ± 8	56	...	...	-28.8 ± 4.0	9.6	...	A0[1]
06083055+2629408	HD 252102	9.149	212	3/3	61 ±10	45	...	-55	-22.5 ± 6.7	21.6	...	A0[1]
06084365+2425140	HD 252198	9.829	143	4/4	40 ± 8	88	...	...	-12.5 ± 2.7	51.1	SB1	B9[1]
06085030+2426029	HD 252199	8.975	221	3/3	7 ± 6	20	...	...	5.5 ± 1.8	22.1	SB1	A0 V[1]
06094684+2000065	...	9.667	149	3/3	41 ± 5	41	...	...	-7.8 ±10.0	7.0	...	...
06095646+2414205	HD 252504	8.788	246	4/4	15 ± 4	90	31	-35	-7.6 ± 1.0	4.7	...	B9.5 V[1]
06104483+1149406	...	10.138	83	6/7	43 ± 8	55	...	...	10.9 ± 7.9	20.7	...	...
06110290+1923317	...	9.612	154	3/3	6 ± 4	54	...	-42	19.8 ± 1.4	1.9	...	...
06134099+3230413	HD 253406	9.649	135	12/13	8 ± 4	101	30	-45	23.4 ± 1.2	2.1	...	...
06153947−6617322	HD 44247	7.502	346	1/1	4 ± 4	68	17	...	51.2 ± 1.0	...	...	B9 IV[1]
06182278+0831463	HD 43774	9.234	147	3/4	61 ± 7	50	...	...	11.8 ±10.0	18.7	...	A0[1]
06252689+2154524	HD 44928	8.813	255	3/3	22 ± 6	25	...	-30	10.0 ± 6.7	10.7	...	B9[1]
06302747−0441487	HD 45975	7.580	278	7/7	70 ± 5	53	...	...	20.6 ± 6.2	17.8	...	B8 V HgMn[1]
06355250+0049433	HD 288875	10.118	131	12/12	22 ± 4	84	...	-41	20.6 ± 4.1	4.3	...	A[1]
06364586+1647491	...	10.051	114	11/12	24 ± 5	74	...	-68	0.8 ± 5.1	9.4	...	...
06374581+1824057	HD 47104	7.760	334	12/12	21 ± 5	99	...	-48	4.9 ± 2.0	5.0	...	B8 V[1]
06380778−0243325	HD 295233	10.760	89	3/3	12 ± 4	64	...	...	4.5 ± 7.3	2.4	...	B9[1]
06381871+0559217	HD 47314	8.535	222	22/23	10 ± 6	38	...	-51	20.4 ± 3.7	6.4	...	B8 Ib[1]
06385615−7121097	HD 48877	9.821	82	1/1	18 ± 7	33	...	...	-8.0 ± 4.5	...	...	A1/2IV[1]
06390846+2357204	...	10.880	87	3/3	14 ± 5	51	...	...	28.7 ± 4.4	1.4	...	...
06395080+3455377	BD+35 1461	9.970	130	9/9	18 ± 5	100	...	-24	-17.1 ± 1.6	60.6	SB1*	B8[1]
06402199−0322092	HD 47798	8.408	289	3/3	52 ± 9	44	...	...	27.3 ± 9.1	10.9	SB2	B8 Ib/II[1]
06412748−2422589	HD 48240	8.560	262	3/3	19 ± 5	75	...	-23	19.9 ± 1.9	0.5	...	B8 II[1]
06413903+3401562	HD 47749	9.051	180	8/9	44 ± 7	51	...	...	-13.9 ± 5.6	11.1	...	A0[1]
06494984+1612105	HD 49606	6.135	671	2/6	18 ± 4	24	...	...	6.7 ± 7.3	1.3	...	B8 MnHgSi[2]
06501063−0609191	HD 49843	8.988	222	3/3	49 ± 4	78	...	...	9.3 ± 9.3	3.9	...	B8 II[1]
06550221−1146139	HD 50984	8.284	291	5/5	17 ± 2*	65	...	-43	17.4 ± 1.3	79.5	SB1	B8/9 II/III[1]
06561603−2839053	HD 51459	10.151	123	1/1	5 ± 4	50	30	...	63.0 ± 1.3	...	SB2	B9.5 IV[1]
06572439−0928136	HD 51539	9.657	127	4/4	18 ± 1*	38	...	...	48.1 ± 3.4	9.6	SB2	B9/A0 III[1]
06574190−0853308	HD 51624	9.585	112	3/4	54 ± 7	...	...	...	12.3 ± 7.2	106.7	SB1	B9 III[1]
06592793+2554510	HD 51688	6.625	...	0/6	...	...	...	...	...	...	...	B8 SiMn[2]
06594865−1123532	...	9.769	144	3/3	37 ± 4	84	...	-38	26.6 ± 3.0	4.2	...	...
07003648+0342256	...	10.189	126	12/15	89 ± 4	91	...	...	-4.8 ±10.0	107.1	SB1*	...
07003712−0248297	HD 52310	9.903	111	3/3	74 ± 7	50	...	...	-8.7 ± 5.4	7.0	...	B7/8 Ib[1]
07021738−0422358	HD 296129	10.679	90	3/3	11 ± 5	76	...	-35	22.1 ± 2.3	1.5	...	A2[1]
07022594+0110297	HD 289500	10.077	135	3/3	41 ± 4	84	...	-31	1.5 ± 4.7	6.3	...	A2[1]
07022828−0455134	HD 296171	10.842	74	3/3	17 ±11	30	...	...	18.1 ± 7.3	5.7	...	B9[1]
07024892+0046465	HD 289591	10.519	87	2/3	37 ±11	54	...	...	-3.1 ± 7.3	12.3	...	A0[1]
07041623+0130268	HD 53204	7.664	426	3/3	18 ±10	19	15	-22	57.2 ± 2.2	5.0	...	B9 Si[2]
07075055+0157564	HD 54138	9.918	129	3/3	20 ± 6	70	...	-68	25.5 ± 3.7	4.8	...	B8 Ib[1]
07125401+0042241	HD 55413	8.580	219	3/3	23 ± 7	57	...	-45	7.6 ± 3.7	6.4	...	B9 III[1]
07125548−2813197	CD−28 4012	9.505	166	12/12	45 ± 4	87	...	...	14.9 ± 5.4	23.5	...	...
07140119−1009028	HD 55776	10.017	113	6/6	10 ± 1*	105	...	-39	15.7 ± 1.3	49.5	SB1*	B8 II[1]
07143511−1019002	NGC 2353 143	11.830	45	5/5	21 ± 4	44	...	...	46.4 ± 8.0	8.9	...	...
07144161−1017068	NGC 2353 108	10.366	90	6/6	6 ± 4*	48	...	...	16.2 ± 2.6	85.2	SB2*	...

[1] SIMBAD
[2] Renson 2009

Table 4 – *continued*

2MASS Designation	Other Name	2MASS H (mag)	<S/N>	$N_{RV}/N_{obs.}$	$v \sin i$ (km s^{-1})	$<W_\lambda>$ Mn II 15413 (mÅ)	$<W_\lambda>$ Ce III 15961 (mÅ)	$<W_\lambda>$ C I 16895 (mÅ)	<RV> (km s^{-1})	$RV_{scat.}$ (km s^{-1})	Binary Type	Literature Spectral Type
07165331+0707153	HD 56331	9.313	165	16/16	11 ± 5	75	...	-52	11.1 ± 1.5	4.5	...	B9[1]
07173234−0509450	HD 56611	9.393	165	4/4	25 ± 5	52	...	-46	12.2 ± 3.1	2.9	...	B9 II/III[1]
07201647+1413206	none	9.170	188	3/3	30 ± 6	55	...	...	2.1 ± 3.5	3.5	...	...
07211999−0618255	HD 57500	9.803	141	4/4	14 ± 6	60	...	...	9.1 ± 3.2	1.3	...	B9 IV[1]
07333287−1217103	HD 60338	9.211	236	3/3	37 ±11	62	...	...	11.9 ± 5.4	18.0	...	B9 II/III[1]
07355974−2530427	HD 60954	9.139	167	1/1	9 ±11	9	...	...	7.3 ± 3.5	...	...	B3V[1]
07391224−2526432	HD 61619	8.522	184	1/1	44 ± 8	106	...	...	18.7 ± 1.3	...	...	B8/9 II[1]
07532177+2527295	HD 64126	9.919	120	7/7	46 ± 9	47	...	...	20.3 ± 4.2	13.8	...	A0[1]
08162588+3533025	none	8.042	331	4/4	14 ± 4	21	...	...	-5.8 ± 6.8	59.6	SB1	...
09432220−5348264	HD 298641	10.311	111	3/3	5 ± 5	42	...	...	16.4 ± 2.7	48.5	SB2	A2[1]
10491776−5943197	...	8.919	277	1/1	40 ±11	40	...	...	-5.3 ± 5.9	...	...	...
12142202+4702530	HD 106420	8.478	284	2/2	50 ± 4	27	...	-42	0.3 ± 6.3	6.8	...	B7 V[1]
14482274−5959316	HD 130039	9.603	161	2/2	21 ±11	26	...	...	-97.8 ± 7.2	203.7	SB2	B6/7[1]
14504493−6001097	none	10.183	111	3/3	14 ±11	53	...	...	-31.7 ± 3.8	5.3	...	...
15525475−4937047	HD 141765	8.563	225	6/6	35 ±11	45	...	...	-40.3 ± 5.6	131.4	SB1	B9 IV[1]
16131358−5135499	HD 145396	9.734	125	2/2	18 ±11	37	...	...	-83.1 ±10.0	87.0	SB1	B7/8 II/III[1]
16133258−6019519	...	10.289	90	9/11	11 ± 4	15	...	...	7.2 ± 5.1	14.4	SB2?	...
16462850−0154589	NGC 6218 K 2	10.530	98	6/9	9 ± 4	34	...	...	8.3 ± 2.6	31.0	SB1*	...
17122286+5713243	HD 156127	8.425	210	46/46	27 ± 8	37	28	-47	-2.9 ± 3.4	11.7	...	B9[1]
17154842+5604392	HD 156678	8.621	181	2/4	20 ± 4	10	...	...	-8.0 ± 5.2	6.8	...	A0[1]
17190217−4841476	HD 156275	7.849	350	8/8	32 ± 8	41	...	...	-2.3 ± 4.3	13.8	...	B9 III/IV[1]
17314436−2616112	HD 158704	6.196	635	4/4	3 ± 1*	39	...	...	-4.9 ± 0.7	1.5	SB2	B9 MnHg[2]
17372735−2547329	none	10.872	64	2/2	11 ± 4	49	...	...	-17.3 ± 4.0	2.1	...	...
17424373−2310270	...	10.644	79	3/3	19 ± 5	39	...	...	-7.3 ± 7.8	1.8	...	...
17533356−2109150	HD 162779	8.270	242	6/6	27 ± 3*	76	...	-41	-1.3 ± 2.9	44.0	SB1*	B5/7 (Ib+O
17582421−2915479	HD 163632	8.966	176	2/2	19 ± 7	44	...	...	-44.5 ± 2.5	19.5	SB1	B9 III[1]
17592288−4812107	HD 163581	10.204	105	8/8	13 ± 5	30	...	-56	-8.6 ± 2.8	5.7	...	A2[1]
18033334−0752452	BD−07 4553	9.570	118	14/15	29 ± 4	97	...	-55	-11.5 ± 2.3	6.4	...	...
18064814−2902119	HD 165347	8.092	241	11/11	26 ± 5	63	...	-75	-35.4 ± 3.2	10.0	SB2	A0 II/III[1]
18071622−1533239	HD 165576	8.402	187	3/3	32 ± 7	29	...	...	-14.3 ± 1.9	12.8	...	B8 Si[2]
18132239−2108047	...	10.678	86	1/1	39 ± 8	95	...	...	-2.1 ± 7.5	...	...	...
18145139−1440361	ALS 9426	10.440	122	1/1	15 ± 4	58	39	...	-2.5 ± 7.0	...	...	B[1]
18155826−1310062	...	10.829	93	1/1	27 ± 7	28	22	...	-4.1 ± 6.4	...	...	...
18165873+6844292	HD 169027	6.955	461	1/1	...	...	...	...	-19.7 ±10.0	...	...	A0 Mn[2]
18174890−1613533	...	10.515	121	1/1	10 ± 7	42	...	...	8.2 ± 1.4	...	...	...
18185671−1117001	HD 168182	9.069	250	1/1	29 ± 9	37	...	...	-17.2 ± 4.2	...	...	A0[1]
18190665−1114478	...	10.685	110	1/1	31 ± 5	80	...	...	20.4 ± 2.9	...	...	...
18200414−3222032	HD 319293	9.414	148	9/9	51 ±11	63	...	...	-10.3 ± 6.2	19.8	...	B9[1]
18263293−1219480	ALS 9616	10.313	91	4/5	48 ± 6	68	...	...	-9.0 ± 7.5	84.8	SB1	B[1]
18271205−1521119	...	10.272	115	1/1	16 ± 5	33	14	...	80.1 ± 1.0	...	...	...
18273013−2905280	HD 169787	9.376	187	4/4	23 ± 4	124	...	...	-16.8 ± 2.3	2.8	...	B9 III[1]
18320103−1203481	BD−12 5089	9.792	92	2/2	57 ± 8	67	...	...	49.7 ± 7.5	20.5	...	...
18360785−0636525	BD−06 4804	9.943	96	5/6	33 ±12	52	...	-51	-15.1 ± 2.3	6.7	...	B9[1]
18391486+2029512	HD 172397	7.675	323	13/13	25 ± 7*	54	...	...	-21.2 ± 3.4	60.8	SB2*	B8[1]
18433871−0615093	BD−06 4856	10.056	113	5/5	6 ± 5	54	30	-50	-8.1 ± 1.9	4.3	...	B9[1]
18441162+0450192	HD 173274	8.861	220	3/3	26 ± 5	60	...	...	-19.4 ± 2.8	1.4	...	A0[1]
18532091+1716194	HD 229910	9.232	145	6/6	16 ± 7	62	22	-21	-4.3 ± 1.8	1.2	...	A0[1]
18571064−0748258	HD 175752	10.203	96	4/7	36 ± 7	41	...	...	-34.4 ± 3.8	28.9	...	B9 Ib/II[1]
19010208+3332494	HD 176913	8.294	290	6/6	49 ±10	65	...	...	-19.3 ± 3.8	11.1	...	A0[1]
19051157−2104584	HD 177379	8.817	203	8/8	8 ± 4	62	...	...	1.2 ± 1.1	84.8	SB1*	B8/9 IV[1]
19121676−2337224	HD 179135	9.544	121	1/1	36 ± 9	60	...	...	8.4 ± 6.8	...	...	B8/9 III[1]
19140822+2722553	HD 337944	9.110	190	11/13	38 ± 3*	37	...	-39	-21.2 ± 4.0	51.3	SB1*	A0[1]
19192341−1657164	HD 181004	9.560	135	3/3	6 ± 6	97	...	...	1.3 ± 1.2	1.1	...	B9 Si[2]
19194613+6423269	HD 182308	6.739	536	3/3	7 ± 4	82	...	-30	-23.6 ± 1.0	0.7	...	B9 HgMn[2]
19223868+1433117	HD 231263	8.310	334	11/11	18 ± 2*	40	...	...	-4.2 ± 3.3	140.9	SB2*	A2[1]
19241521+1803224	HD 231319	8.601	255	3/3	5 ± 4	35	...	-43	-24.6 ± 1.1	6.7	SB1	A0[1]
19255695−0003222	none	10.478	93	5/7	39 ± 7	67	...	...	10.8 ± 4.7	25.6	...	...
19292104+2631356	HD 338459	9.187	206	12/12	24 ± 4	36	...	-37	-6.4 ± 2.9	16.0	...	A2[1]
19294289+2513409	HD 338483	8.964	231	12/12	14 ± 4	64	...	-40	-19.8 ± 2.3	3.8	...	B9[1]
19294384−1801510	HD 183327	9.570	156	1/1	12 ± 5	47	...	...	4.3 ± 2.1	...	SB2	B(8) IV/V[1]
19302877−0716248	HD 183566	9.244	204	2/3	34 ± 6	44	...	...	35.7 ± 5.6	5.1	...	B8 II[1]
19330365+0710372	BD+06 4185	10.368	114	3/3	18 ± 5	57	...	...	4.8 ± 3.4	3.9	...	A0[1]
19334968+4128452	KIC 6128830	9.359	161	29/29	25 ± 5	83	...	-18	0.9 ± 1.1	9.2	...	B6[1]
19384811−0333211	HD 185358	8.413	271	6/6	14 ± 6	34	...	-41	2.2 ± 2.0	1.6	...	B9 III[1]
19413927+4038339	HD 186254	8.578	192	26/26	20 ± 4	46	36	...	-27.6 ± 3.0	8.9	...	B6 III[1]
19421487+2415408	HD 344757	9.458	155	32/33	48 ± 6	64	...	...	-22.0 ± 4.3	125.7	SB1*	B9[1]
19451699+2237253	HD 344908	9.159	154	38/38	15 ± 4	97	...	-32	-11.8 ± 1.0	3.9	...	B8[1]
19454054+3959248	HD 225692	9.310	122	16/16	9 ± 2*	38	...	-24	-7.7 ± 2.3	37.1	SB2*	B8[1]
19455135+2237403	...	10.603	73	11/36	25 ± 4	55	...	...	-0.7 ±10.0	19.3	...	...
19471097+3314589	HD 225783	10.190	126	3/3	5 ± 4	34	...	-65	8.8 ± 2.5	5.0	...	...

[1] SIMBAD
[2] Renson 2009

Table 4 – *continued*

2MASS Designation	Other Name	2MASS H (mag)	<S/N>	$N_{RV}/N_{obs.}$	$v \sin i$ (km s^{-1})	$<W_\lambda>$ Mn II 15413 (mÅ)	$<W_\lambda>$ Ce III 15961 (mÅ)	$<W_\lambda>$ C I 16895 (mÅ)	<RV> (km s^{-1})	$RV_{scat.}$ (km s^{-1})	Binary Type	Literature Spectral Type
19473569+3230397	HD 331252	9.175	210	3/3	7 ± 5	50	...	...	-1.6 ± 1.5	23.4	SB1	B8[1]
19541074+0525290	HD 188265	9.061	249	3/3	22 ±10	47	...	-66	1.3 ± 1.4	3.3	...	A0[1]
19575504+1849260	HD 351059	10.519	93	5/6	41 ±10	79	...	...	0.2 ± 6.8	20.4	...	A0[1]
20003099+0557424	HD 189579	10.161	103	3/3	25 ± 6	40	...	...	-4.0 ± 4.8	13.5	...	B8[1]
20044866+0943598	HD 190494	9.259	140	6/6	51 ± 7	72	...	...	-15.1 ± 6.6	32.8	...	B8[1]
20105316+2849570	HD 191835	9.189	194	3/3	57 ± 7	90	...	...	-14.7 ± 7.9	14.3	...	A0[1]
20151242+3836317	HD 192766	7.895	197	2/2	17 ± 8	12	...	...	2.2 ±10.0	4.1	...	B9 IV[1]
20170054+3557266	HD 193064	7.721	299	4/4	11 ± 5	44	...	-47	-32.2 ± 1.3	2.0	...	A0[1]
20195616+2856578	...	9.291	199	3/3	71 ±10	66	...	...	19.3 ± 4.9	26.5	...	...
20243656+3848339	none	11.857	68	1/1	22 ±11	63	...	...	22.5 ± 3.1	...	...	...
20302325+4039530	HD 195529	8.139	286	9/9	22 ± 1*	44	...	...	-12.1 ± 1.9	27.8	SB1*	A0[1]
20324350+3916157	HD 195918	8.459	244	6/6	67 ± 8	75	...	...	-0.1 ± 5.7	43.4	...	B9[1]
20360994+3929487	BD+38 4160	9.352	151	9/9	13 ± 3*	48	...	...	-24.5 ± 3.0	48.4	SB2*	A0[1]
20422121+6321036	HD 197751	7.533	308	13/13	29 ± 1*	58	27	-64	-16.4 ± 3.8	41.5	SB1*	B8[1]
20425774+3400092	...	10.588	93	2/3	28 ± 8	28	...	...	-8.6 ± 4.1	10.3	...	...
20430277+3403379	...	10.754	86	3/3	31 ±10	50	...	...	-17.2 ± 6.3	20.0	...	...
20452976+5046478	HD 235352	9.207	152	12/12	19 ± 1*	91	41	-38	-15.6 ± 2.1	10.9	...	B8 V[1]
20460258+5135078	...	10.530	89	11/12	20 ± 5	55	...	-31	-10.4 ± 3.3	7.0	...	...
20510469+5025102	...	10.426	111	5/5	15 ± 5	47	...	...	-0.4 ± 2.9	5.2	...	...
20545669+3941137	BD+39 4364	9.540	154	3/3	4 ± 4	56	...	-47	-13.8 ± 1.4	1.3	...	B8 III[1]
21123116+3201498	HD 202033	8.512	127	12/12	8 ± 5	33	...	-65	-12.0 ± 4.9	4.0	...	B9[1]
21151673+3229008	BD+31 4388	9.120	140	12/12	18 ± 4	32	...	...	-24.4 ± 2.9	6.3	...	A0[1]
21292940+4638260	...	10.194	101	14/16	8 ± 4	55	...	-33	-11.8 ± 2.0	3.7	...	...
21293155+6712545	...	10.696	103	3/3	34 ± 5	47	...	...	-22.1 ± 8.3	14.9	...	...
21343477+6728477	...	10.104	143	3/3	29 ± 5	94	42	-49	-22.0 ± 2.0	41.1	SB1	...
21361082+5058585	...	10.774	79	11/13	44 ± 8	72	...	...	-29.1 ± 5.5	18.4	...	...
21402036+5309063	...	9.728	153	3/3	20 ± 6	65	...	...	-5.6 ± 1.4	4.7	...	...
21510496+3932119	HD 207857	6.331	587	3/3	13 ± 1*	77	32	-43	-9.7 ± 1.1	1.6	...	B8 Hg Mn[2]
21592999+1539417	HD 208963	8.400	227	4/4	12 ± 6	36	...	...	-12.9 ± 1.9	3.5	...	A0[1]
22032307+5129046	...	10.543	97	3/3	29 ± 6	75	...	-77	-31.6 ± 3.7	6.2	...	...
22094417+5723120	HD 239872	8.587	198	1/1	20 ±11	58	46	...	4.0 ± 3.4	...	...	B8 Si[2]
22171204+4058047	BD+40 4771	9.387	184	7/7	14 ± 1*	52	...	-31	-26.0 ± 2.1	36.9	SB1*	A0[1]
22193942+5254413	...	10.119	131	3/3	36 ± 8	51	...	...	-3.8 ± 2.5	67.8	SB1	B8[1]
22202642+5541031	HD 212093	8.357	198	2/2	8 ± 5	53	28	...	-22.5 ± 1.6	2.0	...	B9[1]
22210388+5559088	HD 212183	8.144	218	2/2	13 ± 5	83	...	...	-19.6 ± 1.1	0.1	...	B9 III-IV[1]
22222759+5129071	HD 235814	9.368	183	3/3	23 ± 8	72	...	-36	-24.0 ± 1.8	2.1	...	B8[1]
22253247+5330180	...	10.709	92	3/3	41 ± 7	91	...	...	-34.0 ± 5.2	4.4	...	B8[1]
22434824+4554327	HD 215356	9.545	165	12/12	21 ± 9	23	...	...	2.7 ± 4.2	152.6	SB1*	A0[1]
22511031+5355112	HD 216328	8.305	307	3/3	38 ±10	53	...	-63	-27.9 ± 6.1	8.7	...	A0[1]
22551969+5342458	BD+52 3325	9.432	161	3/3	6 ± 4	24	...	-37	-38.1 ± 2.2	3.4	...	...
22564862+5132291	HD 236000	9.510	158	3/3	21 ± 5	60	...	-68	-7.3 ± 3.0	3.4	...	A0[1]
22585819+5834091	HD 217334	8.341	348	6/6	14 ± 4	57	31	-63	-9.2 ± 1.5	3.7	...	A0[1]
22593286+6108246	BD+60 2465	8.766	259	3/3	53 ± 6	38	...	...	-4.7 ± 9.1	8.8	...	B8 III[1]
23082677+5530389	...	10.693	96	2/3	23 ± 6	39	...	...	-28.9 ± 4.3	0.6	...	...
23114474+5706320	HD 218981	8.388	267	3/3	48 ± 7	70	...	-26	-29.9 ± 4.5	2.1	...	B8[1]
23143407+5317045	HD 236074	9.316	166	2/3	43 ± 7	61	...	-50	-22.8 ± 4.5	21.2	...	B8[1]
23145892+5456272	HD 219417	8.720	216	3/3	32 ± 9	20	...	-36	-22.9 ± 6.1	18.7	...	A0[1]
23184953+5345593	...	10.358	93	3/3	22 ±10	32	...	...	-22.7 ± 2.4	2.1	...	...
23213706+6356254	...	9.585	135	3/3	10 ± 4	39	...	-42	-6.9 ± 2.9	1.6	...	...
23215234+4321150	BD+42 4649	9.954	130	3/3	10 ± 5	53	...	-42	-4.3 ± 1.9	1.6	...	B8[1]
23241934+5944208	HD 240288	9.440	175	3/3	3 ± 4	101	...	-40	-12.8 ± 1.1	0.9	...	B8[1]
23244540+6011416	HD 240294	9.614	180	3/3	36 ± 4	30	...	...	-9.9 ±10.0	12.2	...	B9 V[1]
23372390+5641158	...	10.140	117	3/3	21 ± 5	69	40	-34	-13.4 ± 3.2	4.4	...	...
23433663+7919489	...	10.766	74	3/4	49 ±12	53	...	...	-36.8 ±10.2	25.7	...	A0[1]
23483171+5546054	HD 240409	9.635	145	8/8	45 ± 4	63	...	...	-32.2 ± 4.2	17.6	...	B3[1]
23494714+5529504	...	10.643	91	5/5	6 ± 4	105	...	...	-36.6 ± 2.0	1.8	...	...
23510455+6100137	ALS 18097	10.325	97	14/15	40 ± 7	68	...	...	-11.9 ± 2.4	7.8	...	B8 III[1]
23575323+5723194	HD 224435	8.173	282	23/23	33 ± 2*	29	...	...	-10.7 ± 4.3	13.4	SB2*	B9[1]

[1] SIMBAD
[2] Renson 2009

APPENDIX A: LONG TABLES

This paper has been typeset from a TEX/LATEX file prepared by the author.

Table A1. Optical Spectroscopy Log

Star	HJD-2.45E5	Exp. Time (s)	Airmass	S/N ~5500 Å
α And	8797.622	5	1.036	353
HD 16727	8872.645	180	1.146	426
Maia	8872.671	60	1.064	390
HD 27295	8569.607	180	1.480	322
μ Lep	8569.590	25	1.893	259
HD 38478	8561.709	200	1.748	322
HD 58661	8561.773	180	1.382	421
HD 75333	8548.632	180	1.433	189
HD 89822	8561.784	120	1.205	295
HD 158704	8673.692	250	2.055	316
	8678.703	250	1.963	261
	8707.603	250	2.027	292
HD 172044	8797.534	200	1.156	292
Vega	8776.684	1	1.749	481
HD 190229	8797.540	200	1.079	290
HD 207857	8707.641	250	1.604	274
HD 211838	8696.831	65	1.362	285
HD 220933	8882.550	180	1.459	235
00364423+5810121	8801.667	1200	1.111	159
00570626+6134007	8678.782	900	2.056	223
	8776.729	900	1.155	190
	8784.772	900	1.150	237
	8797.601	800	1.267	216
	8872.652	900	1.416	207
01191843+5902478	8801.681	900	1.126	234
01590590+6132312	8776.757	800	1.168	312
	8797.628	750	1.310	258
	8872.664	700	1.307	300
02030138+6103545	8797.729	1100	1.143	138
02183895+5622346	8797.697	800	1.143	210
	8872.719	750	1.443	230
02232391+5651153	8776.769	900	1.130	264
	8797.672	900	1.203	225
	8872.730	800	1.483	218
02261624+5704069	8797.640	1000	1.306	293
	8872.742	900	1.540	238
	8882.594	900	1.137	213
03140847+4007085	8776.796	600	1.062	335
	8797.718	600	1.106	256
	8872.639	500	1.035	334
	8882.584	500	1.013	227
04502564+6328354	8776.782	1200	1.403	197
	8784.793	1200	1.302	221
04510073+3226501	8783.981	1200	1.075	181
	8797.766	1200	1.183	129
04572691+3010291	8882.659	1200	1.005	183
05362280+3219581	8872.769	900	1.077	280
05380741+2418520	8913.675	1200	1.152	165
05400356+3153578	8913.690	800	1.182	247
05542138+5215443	8882.783	800	1.189	172
06070692+2303141	8913.786	900	1.889	188
06550221−1146139	8882.712	700	1.407	162
	8913.755	700	2.035	195
06572439−0928136	8882.725	1200	1.351	150
07140119−1009028	8913.742	1400	1.644	146
07144161−1017068	8784.016	601	1.374	103
17533356−2109150	8673.718	1200	1.767	137
	8678.774	1200	1.743	152
18391486+2029512	8673.730	800	1.073	251
	8678.722	500	1.061	227
	8696.854	800	1.392	225
	8707.612	600	1.129	252
	8782.546	700	1.096	294
	8797.555	700	1.288	239
19140822+2722553	8673.755	1200	1.051	248
	8678.743	1000	1.047	204
19223868+1433117	8673.772	1200	1.090	173
	8696.841	1200	1.202	141
	8767.593	1500	1.075	205
	8776.696	1400	1.810	181
	8782.560	1400	1.089	193
19454054+3959248	8673.786	1200	1.035	209
	8707.656	1200	1.102	202
	8797.570	1100	1.099	173
20302325+4039530	8673.740	900	1.223	264
	8678.730	800	1.209	248
	8696.865	900	1.070	256
20360994+3929487	8678.756	1100	1.138	173
	8776.741	1200	1.431	195
	8782.666	1200	1.149	212
20422121+6321036	8673.794	1200	1.211	192
	8707.619	600	1.430	261
20452976+5046478	8707.670	1053	1.201	180
22171204+4058047	8696.878	1200	1.011	200
23575323+5723194	8773.796	736	1.148	229
	8775.762	850	1.115	213

Table A2. SB1 Orbital Solutions

2MASS ID	N_{RV}	P (d)	$T_{max.RV}$ (HJD-2.45E5)	e	ω (deg.)	γ (km s^{-1})	K_1 (km s^{-1})	$a_1 sini$ (AU)	$f[M_1,M_2]$ ($M_\odot$)	χ^2
01590590+6132312	9	21.794±0.007	5791.904±0.864	0.000±0.000	90.000±0.000	−7.416±0.402	12.480±0.611	0.025±0.001	0.004±0.001	6.081
02232391+5651153	12	14.565±0.001	5805.879±0.235	0.413±0.031	201.647±3.774	−7.098±0.379	15.514±0.517	0.019±0.001	0.004±0.001	17.423
03140847+4007085	10	30.456±0.003	5809.752±0.056	0.720±0.048	333.549±4.412	7.462±0.440	36.576±5.721	0.071±0.012	0.052±0.029	1.909
05014768+2146215	8	42.634±0.024	5798.451±0.460	0.000±0.000	90.000±0.000	2.570±1.647	45.705±3.063	0.179±0.012	0.422±0.085	3.118
05362280+3219581	8	16.109±0.001	5796.707±0.113	0.323±0.033	148.052±3.275	−2.315±0.730	46.344±1.040	0.065±0.002	0.141±0.018	1.448
05403287+3311244	9	54.717±0.141	5786.653±3.092	0.000±0.000	90.000±0.000	−11.192±1.024	15.389±2.491	0.077±0.013	0.021±0.010	3.665
05530948+2654242	10	18.507±0.024	5796.129±1.485	0.000±0.000	90.000±0.000	−12.862±0.856	19.105±1.210	0.033±0.002	0.013±0.003	3.647
05542138+5215443	8	34.707±0.016	5777.021±1.069	0.000±0.000	90.000±0.000	−24.348±0.568	6.800±1.065	0.022±0.003	0.001±0.001	7.340
06051550+3045489	15	39.714±0.030	5763.395±0.829	0.488±0.034	8.508±6.811	−16.222±0.506	18.975±1.081	0.060±0.004	0.019±0.004	3.559
06395080+3455377	9	4.701±0.000	5798.665±0.037	0.000±0.000	90.000±0.000	−14.682±0.645	30.296±0.762	0.013±0.000	0.014±0.001	1.787
07003648+0342256	12	3.820±0.001	5798.888±0.088	0.000±0.000	90.000±0.000	3.773±3.177	44.994±4.977	0.016±0.002	0.036±0.012	13.570
07140119−1009028	6	22.690±0.009	5784.093±1.042	0.449±0.052	32.023±8.620	5.998±1.342	23.531±1.350	0.044±0.003	0.022±0.006	2.642
16462850−0154589	6	7.056±0.006	5799.671±1.200	0.000±0.000	90.000±0.000	−0.303±1.117	19.308±2.442	0.013±0.002	0.005±0.002	1.546
17533356−2109150	6	49.240±0.056	5770.478±1.871	0.000±0.000	90.000±0.000	2.490±1.749	23.324±2.371	0.106±0.011	0.065±0.020	1.876
19051157−2104584	8	4.433±0.000	5800.286±0.082	0.000±0.000	90.000±0.000	−0.495±0.377	46.238±0.549	0.019±0.000	0.045±0.002	5.314
19140822+2722553	11	158.794±0.379	5691.573±4.639	0.000±0.000	90.000±0.000	−29.031±1.510	19.420±1.766	0.283±0.026	0.121±0.033	8.389
19421487+2415408	32	38.311±0.013	5776.054±0.298	0.412±0.013	34.338±2.492	−13.234±0.550	60.766±0.922	0.195±0.003	0.673±0.043	17.433
20302325+4039530	9	11.355±0.002	5800.405±0.519	0.346±0.053	290.022±2.155	−11.637±0.427	17.125±0.420	0.017±0.001	0.005±0.001	8.539
20422121+6321036	13	100.563±0.171	5748.877±3.348	0.000±0.000	90.000±0.000	−14.690±0.969	19.122±0.966	0.177±0.009	0.073±0.011	9.678
22171204+4058047	7	28.792±0.012	5794.822±1.176	0.000±0.000	90.000±0.000	−26.608±1.170	18.614±0.831	0.049±0.002	0.019±0.003	3.180
22434824+4554327	12	5.808±0.000	5799.736±0.056	0.000±0.000	90.000±0.000	−4.978±1.057	78.317±1.228	0.042±0.001	0.289±0.014	6.719

Table A3. Orbital Solutions for SB2s and SB3s

2MASS ID	N_{RV}	P (d)	$T_{max.RV}$ (HJD-2.45E5)	e	ω (deg.)	γ (km s^{-1})	$K_{1,2}$ (km s^{-1})	$a_{1,2} sini$ (AU)	$M_{1,2} sini^3$ ($M_\odot$)	χ^2
00570626+6134007A	10	158.426±0.085	5853.884±1.769	0.551±0.551	346.451±2.515	−7.448±0.430	40.703±2.886	0.495±0.037	5.621±0.978	29.580
00570626+6134007B	10	158.426±0.085	5853.884±1.769	0.551±0.551	346.451±2.515	−7.448±0.430	59.114±3.998	0.718±0.052	3.870±0.649	29.580
02261624+5704069A	13	4.527±0.000	5798.103±0.071	0.080±0.080	61.463±4.823	−6.705±0.428	64.129±0.436	0.027±0.000	1.823±0.056	19.628
02261624+5704069B	3	4.527±0.000	5798.103±0.071	0.080±0.080	61.463±4.823	−6.705±0.428	118.139±1.548	0.049±0.001	0.990±0.020	19.628
04502564+6328354A	11	4.334±0.000	5798.698±0.019	0.000±0.000	90.000±0.000	−4.634±0.705	70.442±1.548	0.028±0.001	1.378±0.043	21.919
04502564+6328354B	11	4.334±0.000	5798.698±0.019	0.000±0.000	90.000±0.000	−4.634±0.705	102.545±1.214	0.041±0.000	0.946±0.040	21.919
04510073+3226501A	9	23.405±0.002	5779.814±0.217	0.417±0.417	55.914±1.786	11.356±0.463	70.006±0.765	0.137±0.002	3.126±0.288	12.952
04510073+3226501B	2	23.405±0.002	5779.814±0.217	0.417±0.417	55.914±1.786	11.356±0.463	78.182±3.372	0.153±0.007	2.799±0.154	12.952
07144161−1017068A	6	9.251±0.004	5800.291±0.845	0.000±0.000	90.000±0.000	13.587±0.912	52.587±2.503	0.045±0.002	1.202±0.175	1.275
07144161−1017068B	3	9.251±0.004	5800.291±0.845	0.000±0.000	90.000±0.000	13.587±0.912	75.916±4.876	0.065±0.004	0.832±0.096	1.275
18391486+2029512A	13	35.378±0.013	5821.247±1.349	0.357±0.357	235.924±7.275	−17.055±0.966	31.385±1.804	0.095±0.006	1.000±0.213	4.338
18391486+2029512B	6	35.378±0.013	5821.247±1.349	0.357±0.357	235.924±7.275	−17.055±0.966	50.249±4.562	0.153±0.014	0.625±0.099	4.338
19223868+1433117A	11	6.235±0.000	5797.070±0.026	0.000±0.000	90.000±0.000	−17.065±0.593	74.187±1.026	0.043±0.001	2.744±0.067	10.823
19223868+1433117B	5	…	…	…	…	…	…	…	…	…
19223868+1433117C	11	6.235±0.000	5797.070±0.026	0.000±0.000	90.000±0.000	−17.065±0.593	116.634±1.149	0.067±0.001	1.745±0.048	10.823
19454054+3959248A	16	337.756±1.956	5810.319±4.003	0.352±0.352	243.553±17.223	−3.093±0.703	16.937±1.706	0.492±0.071	2.115±0.823	12.284
19454054+3959248B	3	337.756±1.956	5810.319±4.003	0.352±0.352	243.553±17.223	−3.093±0.703	31.467±3.093	0.914±0.130	1.139±0.428	12.284
20360994+3929487A	9	31.422±0.012	5774.023±0.576	0.582±0.582	112.929±3.548	−27.390±0.666	23.770±1.990	0.056±0.005	0.358±0.057	11.305
20360994+3929487B	9	31.422±0.012	5774.023±0.576	0.582±0.582	112.929±3.548	−27.390±0.666	44.203±2.145	0.104±0.006	0.192±0.036	11.305
18064814−2902119A	11	…	…	…	…	…	…	…	…	
18064814−2902119B	7	5.469±0.000	5789.682±0.210	0.116±0.116	151.162±8.748	−17.647±0.793	68.402±1.515	0.034±0.001	0.707±0.034	7.216
18064814−2902119C	9	5.469±0.000	5789.682±0.210	0.116±0.116	151.162±8.748	−17.647±0.793	68.402±1.515	0.034±0.001	0.704±0.031	7.216
23575323+5723194A	23	…	…	…	…	…	…	…	…	…
23575323+5723194B	23	21.080±0.001	5806.240±0.084	0.456±0.456	234.674±1.625	−7.197±0.930	86.620±2.911	0.149±0.005	…	4.260

Table A4. Radial Velocity Data (Single Stars; only the first 10 shown because otherwise the Latex fails to compile). HJDs with asterisks indicate optical spectra.

2MASS Designation	HJD-2.45E5	RV (km s^{-1})
00091817+7022314	5850.780	-19.7 ± 1.0
	5851.758	-19.8 ± 1.0
	5869.680	-16.8 ± 1.3
	5871.698	-17.3 ± 1.9
	6173.835	-21.3 ± 2.1
	6204.755	-20.2 ± 2.8
	6224.689	-19.5 ± 1.1
	6233.644	-16.6 ± 4.3
	6234.656	-18.2 ± 1.0
	6257.552	-19.1 ± 1.6
	6258.559	-19.3 ± 2.1
	6262.559	-21.0 ± 5.0
00245787+6212255	5822.883	-27.1 ±10.0
	5823.845	-30.5 ± 1.5
	5845.713	-26.9 ± 3.8
	5848.666	-27.8 ± 3.8
	5851.705	-27.4 ± 1.3
	5866.635	-29.0 ± 1.0
	6171.850	-30.6 ± 2.4
	6172.854	-29.9 ± 1.0
	6177.840	-30.4 ± 1.4
	6203.755	-33.9 ± 2.4
	6223.737	-31.5 ± 1.9
00364423+5810121	5849.751	-23.3 ± 1.3
	5850.727	-21.8 ± 8.7
	5867.686	-31.8 ± 2.8
	5868.667	-43.7 ± 9.9
	5876.631	-27.0 ±10.0
	5881.710	-41.7 ±10.0
	6169.860	-30.9 ±10.0
00390709+5558188	6968.736	-20.6 ± 5.4
	7271.868	-21.0 ± 1.8
	7295.783	-21.8 ± 8.3
	7296.794	-21.1 ± 8.7
	7346.687	-21.4 ± 1.1
	7350.619	-23.2 ± 7.1
01011057+6355294	6990.648	-29.0 ± 1.1
	6993.676	-27.8 ± 1.1
	7293.834	-27.7 ± 1.0
01165086+5902504	6260.612	-13.8 ±10.0
	6283.561	-11.1 ± 8.2
	6288.552	-18.9 ±10.0
	6290.554	-18.2 ± 1.4
01191843+5902478	6260.612	-27.5 ± 2.1
	6283.561	-29.6 ± 1.8
	6288.552	-31.1 ± 2.7
	6290.554	-30.4 ± 2.1
	8801.681*	-26.7 ± 1.4
01494647+5653549	5938.579	-35.1 ± 3.8
	6286.569	-29.4 ±10.0
	6560.833	-30.8 ± 5.1
01533081+5736078	5938.580	-57.0 ± 1.9
	6286.569	-50.3 ± 7.3
	6560.833	-51.5 ±10.0
01590590+6132312	6911.903	4.8 ± 3.3
	6934.831	5.8 ± 2.4
	6935.802	4.0 ± 1.0
	6937.804	3.5 ± 2.0
	6938.795	2.0 ± 1.4
	6968.793	-17.4 ± 3.5
	8776.757*	-20.4 ± 0.8
	8797.628*	-17.0 ± 0.9
	8872.664*	0.6 ± 0.8

Table A4 – *continued*

2MASS Designation	HJD-2.45E5	RV (km s^{-1})
02030138+6103545	6911.903	-23.6 ± 9.8
	6934.831	-8.4 ± 5.3
	6935.802	-0.4 ± 1.3
	6937.804	-25.4 ±10.0
	6938.795	-24.4 ± 9.8
	6968.793	-5.7 ±10.0
	8797.729*	-11.8 ± 3.3
02060290+5009136	5851.812	-34.2 ± 5.3
	5854.830	-33.8 ± 6.9
	5869.747	-42.1 ± 3.6
	5872.777	-42.0 ±10.0
02063211+6056171	6911.903	-9.0 ± 1.7
	6934.831	-9.0 ± 1.3
	6935.802	-7.5 ± 1.0
	6937.804	-9.1 ± 1.0
	6938.795	-7.5 ± 1.1
	6968.793	-8.6 ± 1.0
02154357+5607505	5932.563	-33.6 ± 3.7
	6235.714	-35.4 ± 4.3
	6259.623	-36.9 ± 3.3
02203397+6023494	5844.825	-20.2 ± 4.8
	5850.833	-16.0 ± 5.5
	5871.754	-9.5 ± 1.8
	7650.874	-25.8 ± 4.2
	7677.806	-24.4 ± 2.7
	7710.765	-11.8 ± 1.8
	7762.626	-18.9 ± 3.7
	7764.604	-4.1 ± 3.1
	7766.633	-22.3 ± 3.1
	8008.987	-5.8 ± 1.7
	8037.888	-18.2 ± 5.5
02231800+5903056	7681.817	-14.9 ± 2.2
	7734.624	-13.3 ± 1.6
	7762.561	-15.4 ± 1.0
	7765.575	-18.4 ± 1.0
	8007.893	-19.9 ± 1.1
	8010.892	-14.8 ± 1.0
	8039.832	-11.0 ± 1.2
	8056.760	-17.5 ± 2.9
	8061.812	-19.6 ± 5.9
	8084.690	-16.2 ± 1.1
02232391+5651153	7681.817	0.6 ± 1.0
	7734.624	-18.8 ± 1.0
	7762.561	-29.0 ± 1.0
	7765.575	-3.7 ± 1.3
	8039.833	-25.6 ± 1.0
	8056.760	-4.5 ± 1.0
	8061.812	0.5 ± 1.0
	8064.790	-6.0 ± 1.0
	8084.690	-12.3 ± 1.0
	8776.769*	0.2 ± 0.8
	8797.672*	-21.9 ± 0.8
	8872.730*	0.6 ± 0.8

Table A5. SB2 Radial Velocity Data. HJDs with asterisks indicate optical spectra.

2MASS Designation	HJD-2.45E5	RV_1 (km s^{-1})	RV_2 (km s^{-1})
00570626+6134007	6990.648	-4.3 ± 2.6	-15.0 ± 3.0
	6993.676	-12.3 ± 3.2	-12.1 ± 3.0
	7293.834	11.3 ± 2.8	-47.2 ± 2.5
	7294.829	15.8 ± 2.7	-43.7 ± 2.5
	7297.799	6.6 ± 2.0	-39.8 ± 5.2
	8678.782*	-10.5 ± 2.7	4.7 ± 1.5
	8776.729*	-24.5 ± 1.4	17.4 ± 1.2
	8784.772*	-25.1 ± 1.4	18.6 ± 1.6
	8797.601*	-25.6 ± 1.3	20.0 ± 1.2
	8872.652*	36.9 ± 1.7	-62.9 ± 2.0
02060290+5009136	5851.812	-34.2 ± 5.3	-31.3 ±10.0
	5854.830	-33.8 ± 6.9	-31.8 ±10.0
	5869.747	-42.1 ± 3.6	...
	5872.777	-42.0 ±10.0	-20.4 ±10.0
02203397+6023494	5844.825	-20.2 ± 4.8	-17.4 ± 1.9
	5850.833	-16.0 ± 5.5	-18.2 ± 1.4
	5871.754	-9.5 ± 1.8	-25.2 ± 4.9
	7650.874	-25.8 ± 4.2	-16.4 ± 1.7
	7677.806	-24.4 ± 2.7	-17.0 ± 1.9
	7710.765	-11.8 ± 1.8	-19.0 ± 3.5
	7762.626	-18.9 ± 3.7	-18.3 ± 2.4
	7764.604	-4.1 ± 3.1	-19.7 ± 2.3
	7766.633	-22.3 ± 3.1	-20.9 ± 5.6
	8008.987	-5.8 ± 1.7	-23.2 ± 4.0
	8037.888	-18.2 ± 5.5	-20.4 ± 5.4
02261624+5704069	7681.817	-40.5 ± 2.1	...
	7734.624	-40.1 ± 1.6	...
	7762.561	-67.5 ± 1.5	...
	7765.575	27.7 ± 2.3	...
	8007.893	-26.8 ± 2.1	...
	8010.893	-52.6 ± 1.2	...
	8039.833	0.4 ± 4.3	...
	8056.760	-67.3 ± 2.0	...
	8061.812	-52.8 ± 1.5	...
	8084.690	-34.1 ± 1.7	...
	8797.640*	27.2 ± 1.8	-78.1 ± 1.8
	8872.742*	-9.8 ± 1.5	-2.9 ± 1.2
	8882.594*	48.3 ± 0.9	-106.6 ± 1.3
04315476+2138086	8887.601	-39.0 ± 9.3	110.2 ±10.9
04502564+6328354	6936.927	39.9 ± 5.7	-67.4 ± 2.6
	6942.936	-75.8 ± 5.3	95.6 ± 2.8
	6972.851	-73.9 ± 5.4	88.7 ± 1.9
	7022.730	58.0 ± 7.5	-104.0 ± 3.6
	7058.646	7.3 ± 5.6	-17.3 ± 3.7
	7281.001	-76.2 ± 5.8	97.3 ± 4.4
	7293.008	-41.4 ± 7.7	31.4 ± 4.0
	7296.004	60.4 ± 3.3	-112.3 ± 4.6
	7320.957	4.8 ± 1.5	-7.1 ± 3.0
	8776.782*	-29.9 ± 1.8	30.6 ± 1.6
	8784.793*	-72.0 ± 2.0	93.0 ± 2.1
04510073+3226501	6993.855	97.2 ± 1.0	...
	7359.877	-0.2 ± 1.0	...
	7377.685	-35.0 ± 3.6	...
	7407.720	12.0 ± 2.6	...
	7410.590	40.7 ± 2.0	...
	7651.932	11.0 ± 1.3	...
	7654.930	-42.1 ± 1.3	...
	8783.981*	-20.9 ± 1.5	52.9 ± 1.9
	8797.766*	59.0 ± 1.7	-37.3 ± 2.0
05380741+2418520	6291.688	-29.3 ± 6.9	...
	6559.992	85.8 ±10.0	-80.1 ± 4.4
	6586.929	-20.5 ± 9.7	...
	8913.675*	-33.6 ± 1.9	103.6 ± 1.5
06402199−0322092	6584.981	22.0 ±10.0	21.0 ± 6.0
	6589.999	27.1 ±10.0	23.5 ± 4.2
	6641.838	32.9 ± 7.2	21.8 ± 5.0
06561603−2839053	7830.544	63.0 ± 1.3	-78.7 ± 3.8

Table A5 – *continued*

2MASS Designation	HJD-2.45E5	RV_1 (km s^{-1})	RV_2 (km s^{-1})
06572439−0928136	6587.985	50.9 ± 4.5	41.1 ± 1.7
	6593.990	47.4 ± 1.0	43.5 ± 4.5
	6637.843	51.9 ± 3.0	42.4 ± 4.4
	8882.725*	42.3 ± 5.0	57.8 ± 5.0
07144161−1017068	8027.889	-7.2 ± 3.6	38.5 ± 4.6
	8030.875	-21.0 ± 2.9	...
	8054.853	23.5 ± 1.0	-0.7 ± 2.8
	8058.862	-17.4 ± 3.5	...
	8090.816	55.3 ± 2.9	...
	8784.016*	64.1 ± 1.6	-59.7 ± 1.9
09432220−5348264	8178.679	12.7 ± 5.7	16.8 ± 3.4
	8181.578	42.5 ± 1.3	-16.4 ± 2.0
	8206.603	-6.1 ± 1.0	29.8 ± 1.4
14482274−5959316	8657.534	4.0 ± 4.3	100.2 ± 5.4
	8677.471	-199.6 ±10.0	-22.8 ± 4.3
	8689.462	...	-133.3 ± 5.9
14504493−6001097	8657.534	-35.1 ± 4.9	-92.3 ± 9.4
	8677.471	-29.9 ± 4.2	-24.8 ± 1.0
	8689.462	-30.2 ± 2.3	...
16133258−6019519	7913.676	9.7 ± 8.0	...
	7974.497	-0.5 ± 3.8	...
	8238.723	4.2 ± 5.3	...
	8265.656	3.3 ± 4.3	...
	8266.646	14.0 ± 2.8	...
	8270.666	7.0 ± 1.8	...
	8294.594	13.1 ± 6.3	...
	8297.540	5.0 ± 3.4	...
	8351.489	9.0 ±10.0	...
17314436−2616112	6461.795	-4.3 ± 1.4	-17.7 ± 2.0
	6470.775	...	8.2 ± 2.1
	8673.692*	-4.7 ± 0.6	11.4 ± 1.6
	8678.703*	-5.7 ± 0.4	-15.3 ± 4.1
	8707.603*	-4.9 ± 0.4	14.1 ± 1.7
18391486+2029512	7094.977	-1.2 ± 2.7	...
	7096.972	8.7 ± 3.3	...
	7112.948	-16.6 ± 3.1	...
	7113.924	-23.1 ± 7.7	...
	7115.901	-26.3 ± 4.6	...
	7116.950	-29.9 ± 6.1	...
	7118.919	-43.5 ± 6.2	...
	8673.730*	-30.5 ± 1.7	12.2 ± 7.9
	8678.722*	-52.1 ± 1.8	35.5 ± 5.6
	8696.854*	1.8 ± 1.4	-49.5 ± 5.3
	8707.612*	-26.4 ± 2.2	3.1 ± 7.1
	8782.546*	-43.5 ± 1.2	23.9 ± 4.3
	8797.555*	6.8 ± 2.2	-59.4 ± 7.6
19294384−1801510	8660.848	4.3 ± 2.1	-8.8 ± 3.8
19454054+3959248	5813.703	-19.2 ± 3.2	...
	5823.727	-19.2 ± 2.2	...
	5840.661	-22.3 ± 2.3	...
	5849.578	-21.1 ± 1.7	...
	5851.649	-24.2 ± 5.2	...
	5866.570	-21.5 ± 1.6	...
	7572.975	-13.1 ± 2.7	...
	7573.975	-8.1 ± 3.5	...
	7574.960	-9.2 ± 3.9	...
	8660.955	9.7 ± 1.0	...
	8673.786*	12.9 ± 1.1	-28.9 ±10.0
	8707.656*	8.9 ± 2.1	-22.3 ±10.0
	8733.784	3.2 ± 1.0	...
	8738.746	3.1 ± 2.2	...
	8766.631	2.5 ± 2.9	...
	8797.570*	-5.1 ± 0.8	1.9 ±10.0

Table A5 – *continued*

2MASS Designation	HJD-2.45E5	RV_1 (km s^{-1})	RV_2 (km s^{-1})
20360994+3929487	6934.640	-55.7 ± 4.5	27.2 ± 2.9
	6937.696	-42.4 ± 3.3	8.8 ± 3.6
	6962.607	-15.1 ± 5.0	-50.2 ± 3.0
	7297.720	-17.4 ± 4.5	-42.1 ± 3.5
	7579.960	-24.2 ± 3.1	-42.6 ± 2.6
	7643.801	-21.2 ± 3.5	-44.4 ± 1.8
	8678.756*	-21.5 ± 0.8	-44.6 ± 3.4
	8776.741*	-15.6 ± 1.0	-50.5 ± 2.7
	8782.666*	-7.3 ± 1.4	-58.5 ± 2.4
22202642+5541031	8476.550	-21.4 ± 1.3	...
	8803.658	-23.5 ± 2.0	...
23575323+5723194	5821.805	-12.8 ± 9.1	12.6 ± 2.5
	5824.776	-11.9 ± 6.3	-18.5 ± 4.0
	5843.751	-9.3 ± 6.8	4.7 ± 1.8
	5844.713	-13.0 ± 7.4	-5.1 ± 3.4
	5874.680	-13.6 ± 4.8	-18.3 ± 3.3
	6257.616	-16.4 ± 4.3	56.2 ± 2.0
	6261.621	-14.8 ± 4.4	35.8 ± 2.1
	6284.558	-13.0 ± 2.2	21.0 ± 3.0
	6643.553	-8.7 ± 3.0	18.1 ± 1.8
	6651.564	-10.0 ± 5.3	-103.4 ± 2.6
	8440.664	-18.5 ± 5.1	-50.8 ± 2.7
	8447.608	-6.8 ± 5.9	32.8 ± 2.5
	8732.875	-5.1 ± 3.6	-8.3 ± 4.3
	8733.843	-8.3 ± 3.9	-20.2 ± 2.2
	8744.826	-8.3 ± 5.7	57.5 ± 4.7
	8766.749	-12.0 ± 1.6	56.9 ± 2.4
	8773.796*	-8.0 ± 1.7	6.3 ± 1.2
	8775.762*	-9.3 ± 3.9	-17.1 ± 2.4
	8776.717*	-6.8 ± 5.6	-28.8 ± 1.8
	8776.741*	-6.4 ± 2.5	-28.4 ± 3.9
	8784.760*	-14.2 ± 2.9	32.0 ± 1.8
	8793.634	-7.7 ± 2.1	16.4 ± 2.4
	8861.638	-11.9 ± 1.5	-40.5 ± 4.8

Table A6. SB3 Radial Velocity Data. HJDs with asterisks indicate optical spectra.

2MASS Designation	HJD-2.45E5	RV_1 (km s^{-1})	RV_2 (km s^{-1})	RV_3 (km s^{-1})
18064814−2902119	6444.859	-33.5 ± 2.8	-73.4 ± 2.3	41.3 ± 2.7
	7949.739	-35.6 ± 2.1	-33.2 ± 2.4	...
	8213.895	-34.4 ± 4.4	54.4 ± 3.2	-87.3 ± 4.2
	8235.882	-36.8 ± 3.9	50.0 ± 2.1	-80.8 ± 2.9
	8236.885	-32.7 ± 3.6	-22.7 ± 3.1	...
	8263.866	-34.4 ± 4.3	...	...
	8273.785	-37.0 ± 2.6	53.6 ± 3.3	-91.5 ± 2.5
	8328.670	-34.6 ± 2.1	53.7 ± 7.7	-90.8 ± 1.6
	8353.675	-37.5 ± 2.6	-76.1 ± 3.0	38.6 ± 3.2
	8655.772	-41.4 ± 3.6	12.2 ± 3.1	...
	8712.570	-31.4 ± 2.7	...	-27.7 ± 2.4
19223868+1433117	6934.576	51.4 ± 1.2	...	-125.7 ± 2.0
	6935.639	46.0 ± 4.3	...	-110.7 ± 5.1
	7144.923	-53.5 ± 2.1	...	39.1 ± 2.6
	7153.918	33.5 ± 4.2	...	-103.3 ± 3.4
	7202.902	57.1 ± 6.8	...	-132.4 ± 2.4
	7292.677	-63.5 ± 3.1	...	55.5 ± 3.1
	8673.772*	33.9 ± 3.2	-9.5 ± 3.3	-94.8 ± 2.4
	8696.841*	-83.7 ± 3.4	-10.2 ± 3.6	88.2 ± 2.8
	8767.593*	47.0 ± 2.7	-5.9 ± 7.7	-117.3 ± 3.2
	8776.696*	-66.7 ± 2.6	-5.5 ± 6.9	66.7 ± 3.5
	8782.560*	-47.3 ± 2.6	-5.6 ± 3.7	29.0 ± 2.6